

# Hall-Effect Thruster Simulations with 2-D Electron Transport and Hydrodynamic Ions

IEPC-2009-114

*Presented at the 31st International Electric Propulsion Conference,  
University of Michigan • Ann Arbor, Michigan • USA  
September 20 – 24, 2009*

Ioannis G. Mikellides,<sup>\*</sup> Ira Katz,<sup>†</sup> Richard R. Hofer<sup>‡</sup> and Dan M. Goebel<sup>§</sup>  
*Jet Propulsion Laboratory, California Institute of Technology, Pasadena, CA, 91109*

**Abstract:** A computational approach that has been used extensively in the last two decades for Hall thruster simulations is to solve a diffusion equation and energy conservation law for the electrons in a direction that is perpendicular to the magnetic field, and use discrete-particle methods for the heavy species. This “hybrid” approach has allowed for the capture of bulk plasma phenomena inside these thrusters within reasonable computational times. Regions of the thruster with complex magnetic field arrangements (such as those near eroded walls and magnet pole pieces) and/or reduced Hall parameter (such as those near the anode and the cathode plume) challenge the validity of the quasi-one-dimensional assumption for the electrons. This paper reports on the development of a computer code that solves numerically the 2-D axisymmetric vector form of Ohm’s law, with no assumptions regarding the rate of electron transport in the parallel and perpendicular directions. The numerical challenges related to the large disparity of the transport coefficients in the two directions are met by solving the equations in a computational mesh that is aligned with the magnetic field. The fully-2D approach allows for a large physical domain that extends more than five times the thruster channel length in the axial direction, and encompasses the cathode boundary. Ions are treated as an isothermal, cold (relative to the electrons) fluid, accounting for charge-exchange and multiple-ionization collisions in the momentum equations. A first series of simulations of two Hall thrusters, the BPT-4000 and a 6 kW laboratory thruster, quantifies the significance of ion diffusion in the anode region and the importance of the extended physical domain on studies related to the impact of the transport coefficients on the electron flow field.

## Nomenclature

$\mathbf{B}$ = magnetic induction field	$\hat{\mathbf{b}}$ = magnetic induction field unit vector
$\mathbf{c}$ = particle thermal (or random) velocity	$\beta_{r(z)} = r(z)$ component of magnetic induction field unit vector
$D$ = mean atomic diameter for xenon	$\Delta A$ = surface area of a finite-element edge
$\mathbf{E}$ = electric field	$\Delta t$ = time increment
$e$ = electron charge	$\epsilon$ = contributions to Ohm’s law from the electron pressure and ion current density
$\mathbf{F}_i$ = total specific force on ions	
$f_i$ = ion velocity distribution function	
$(\dot{f}_i)_c$ = rate of change of $f_i$ due to collisions with other	

<sup>\*</sup> Member of the Technical Staff, Electric Propulsion Group, Ioannis.G.Mikellides@jpl.nasa.gov.

<sup>†</sup> Group Supervisor, Electric Propulsion Group, Ira Katz@jpl.nasa.gov.

<sup>‡</sup> Member of the Technical Staff, Electric Propulsion Group, Richard.R.Hofer@jpl.nasa.gov.

<sup>§</sup> Section Staff, Propulsion and Materials Engineering Section, Dan.M.Goebel@jpl.nasa.gov.

species

$\mathbf{j}_{i(e)}$  = ion (electron) current density

$k_B$  = Boltzmann's constant

$L$  = length of the acceleration channel

$\ln(\Lambda)$  = coulomb logarithm

$m_{i(e)}$  = mass of ion (electron)

$n_{i(e)}$  = number density of ion (electrons)

$n_n$  = number density of atoms (neutrals)

$\hat{\mathbf{n}}$  = normal unit vector

$\dot{n}$  = electron-impact ionization rate

$\dot{n}_{i' \rightarrow i}$  = total ion generation rate for collisions that produce

ion "I" from another heavy particle "i"

$p_{i(e)}$  = ion (electron) pressure

$q_i$  = ion charge (eZ)

$Q^T$  = thermal heating

$\mathbf{R}_{i(e)}$  = ion (electron) drag force density

$r, z$  = radial and axial coordinates

$\hat{\mathbf{r}}, \hat{\mathbf{z}}$  = unit vectors in radial and axial directions

$T_{i(e)}$  = ion (electron) temperature

$t$  = time

$\mathbf{u}_{i(e)}$  = mean velocity of ions (electrons)

$\mathbf{u}_n$  = mean velocity of atoms

$u_{T,i}$  = ion thermal speed  $(2k_B T_i / m_i)^{1/2}$

$\mathbf{v}$  = particle velocity

$Z$  = ion charge state

$\epsilon_0$  = permittivity in vacuum

$\epsilon_s$  = ionization potential of species "s"

$\eta$  = total or effective electrical resistivity

$\eta_{ei}$  = electron-ion (e-i) electrical resistivity

$\eta_0$  = classical electrical resistivity

$\kappa_e$  = electron thermal conductivity

$\lambda_{ii}$  = ion-ion collision mean free path

$\lambda_{in}$  = ion-neutral collision mean free path

associated with charge exchange

$\lambda_{nn}$  = neutral-neutral collision mean free path

$\mu_0$  = classical electron mobility

$\nu_B$  = Bohm collision frequency

$\nu_{ei}$  = electron-ion (e-i) collision frequency

$\bar{\nu}_{ei}$  = total electron-ion (e-i) collision frequency

$\nu_{en}$  = electron-neutral (e-n) collision frequency

$\nu_{en}^I$  = electron-neutral (impact) ionization rate

$\nu_{ew}$  = electron-wall (e-w) collision rate

$\nu_{is}$  = collision frequency of ions with species "s"

$\sigma_{in}$  = ion-neutral charge-exchange collision cross section

$\tau_e$  = coulomb collision relaxation time for electrons

$\tau_{ei}^T$  = thermal equilibration time between electrons

$\tau_i$  = coulomb collision relaxation time for ions

$\phi$  = plasma potential

$\chi$  = magnetic-field potential function

$\psi$  = magnetic-field stream function

$\omega_{ce}$  = electron cyclotron frequency

### Greek Symbols

$\alpha$  = factor that controls the magnitude of the Bohm collision frequency

## I. Introduction

THE numerical simulation of Hall thrusters spans more than two decades. In fact, the first theoretical models of the partially-ionized gas in Stationary Plasma Thrusters (SPT) were reported in the 1970s by Morozov and colleagues.<sup>1,2,3</sup> Hirakawa<sup>4,5,6</sup> developed one of the first numerical models of an SPT in three-dimensions. Electrons and singly-charged ions were simulated using a Particle-In-Cell (PIC) scheme that was combined with a Monte-Carlo Collision model (MCC). The electric field was determined by solving Poisson's equation. A computational approach that has been used extensively in the last two decades or so to simulate the partially-ionized gas in Hall thrusters is to solve the fluid (inertia-less) momentum and energy conservation laws for the electrons but use discrete-particle methods to track the evolution of the heavy species. This "hybrid" approach allowed for the capture of bulk plasma phenomena and ion kinetics in the thruster within reasonable computational times and, as a result, gained considerable popularity. One of the first models to follow this approach was developed by Fife and Martínez-Sánchez.<sup>7</sup> The model, dubbed "HPHall" (Hybrid-PIC Hall), uses a PIC-MCC method for ions in 2-D axisymmetric geometry and it appears that it was the first to reproduce the so-called breathing mode oscillations in Hall thrusters, in two dimensions.<sup>8</sup> Interpretations of these oscillations were provided (around the same time) by Fife and Martínez-Sánchez using an idealized 0-D model,<sup>7,8</sup> and by Boeuf and Garrigues<sup>9</sup> using a 1-D time-dependent model with a hybrid treatment of electrons and ions. In Fife's work, a model for anomalous electron mobility was employed in the original (SPT-70) simulations that was based on Bohm's scaling<sup>10</sup> for the anomalous (or neoclassical) collision frequency,  $\nu_B \sim B/16$ . The precise numerical value used in the simulations was guided by experiments. Since the late 90s HPHall has been used to simulate several other thrusters and, naturally, its numerical and physical models have undergone several improvements and extensions. Recently the model was upgraded to HPHall-2\*\* by Parra and

\*\* All simulation results presented in this paper that are termed as "HPHall" results were generated with the HPHall-2 version of the code as modified at the Jet Propulsion Laboratory [Refs 13, 14].

Ahedo.<sup>11</sup> Additional algorithm advancements including a new erosion sub-model were completed at the Jet Propulsion Laboratory.<sup>12,13,14</sup> A similar hybrid approach has been followed by Fernandez and Cappelli that led to the development of a similar model of Hall thrusters and is reported in Refs 15,16. Hagelaar, *et al.*<sup>17,18</sup> also followed a hybrid approach but instead of Bohm diffusion used empirical parameters to account for additional anomalous electron transport<sup>19</sup> and energy loss phenomena. It is interesting to note that despite the apparent popularity of the hybrid approach in recent years, the earliest attempts to model the heavy species followed purely hydrodynamic formalisms<sup>20</sup> (also reported in Ref. 21). A hydrodynamic approach for all species in the thruster was also applied later in 2-D geometries by Keidar and Boyd.<sup>22</sup>

Because the fundamental principle behind the acceleration of ions in Hall thrusters is based on operating the accelerator at high electron Hall parameter ( $\Omega_e > 100$ ), the diffusion of heat and mass for the electron flow in the direction parallel to the magnetic field is much greater (by  $\sim \Omega_e^2$ ) than that in the perpendicular direction for most of the channel region. This leads to a simplification, the so-called quasi-one-dimensional approximation: streamlines of the magnetic vector field are also lines of constant electron temperature and constant “thermalized” potential  $\phi^* \equiv \phi - T_e \ln(n_e)$ . Numerically, the assumption allows for the solution of the plasma potential and electron temperature in a (quadrilateral) computational cell that is bounded by two adjacent lines of force rather than one with arbitrary dimensions. This is the approach followed in HPHall. Modeling regions of the thruster with complex magnetic field arrangements (such as those near eroded walls and magnets) and/or reduced Hall parameter (such as those near the anode and the cathode plume) challenge the validity of the quasi-one-dimensional assumption for the electrons.

In this paper we present a 2-D computational model of the partially-ionized gas in a Hall thruster that employs the full vector form of Ohm’s law, with no assumptions regarding the rate of electron transport in the parallel and perpendicular directions of the magnetic field. The model is a descendant of OrCa2D, a 2-D computational model of electric propulsion hollow cathodes that employs a mix of implicit and explicit algorithms to solve numerically the conservation laws for the partially-ionized gas in these devices.<sup>23,24</sup> Numerical diffusion due to the large disparity of the transport coefficients in the two directions is evaded by solving the equations in a computational mesh that is aligned with the magnetic field. The employment of field-aligned meshes is a long-standing computational approach (dates back more than 15 yrs) for simulating highly anisotropic plasmas, and is widely used nowadays especially by the sustained fusion energy community<sup>25,26,27,28</sup> (e.g. tokamak divertor technologies), and for a variety of space plasma problems dealing with the propagation of shear Alfvén waves.<sup>29</sup> Also, more recently, field-aligned meshing was employed in early versions of a 2-D model of the discharge chamber in an ion engine.<sup>30</sup> It was found that the complexity of the magnetic field near the ring cusps made the field-aligned-mesh generation technique prohibitively sensitive to small changes in the magnetic field strength or geometry. This made the application of the model for the design and study of a wide range of thruster arrangements cumbersome, so the field-aligned mesh was eventually replaced with a simpler orthogonal mesh.<sup>31</sup>

The fully-2D approach followed here allows for a large physical domain that extends more than five times the thruster channel length in the axial direction, and encompasses the cathode boundary and the axis of symmetry. The main motivation is to extend the solution to regions of the Hall thruster that otherwise could not be modeled accurately due to the quasi-1D assumption. The model also incorporates a new algorithm for the solution of the (collisionless) neutral gas density, based on line-of-sight formulations, that eliminates the inherent statistical fluctuations of conventional particle methods. The approach for the neutral gas is presented in a companion paper<sup>32</sup> and will not be described here. The ions are modeled using a fully hydrodynamic approach that, in addition to the inelastic collision terms associated with the ionization, retain both the ion pressure and the ion-neutral charge-exchange “drag” in the momentum equation.

The paper is organized as follows. Section II provides a description of the physical models and numerical methodologies for the ions (II.A) and electrons (II.B). Section III presents results from numerical simulations of two thrusters, the BPT-4000 and a 6 kW laboratory Hall thruster. The numerical simulations of the BPT-4000 (III.A) have been performed mainly for benchmarking purposes and the results are compared with those from recent HPHall simulations of the same thruster.<sup>13</sup> Preliminary studies to better understand the impact of the imposed Bohm collision frequency in the BPT-4000 benchmark simulations motivated an extended investigation in the 6 kW laboratory thruster; the results from these studies are presented in III.B. For the sake of brevity when comparing results with those from HPHall we refer to the newly-developed model as *Hall 2De* (with “2De” referring to electron flow in two dimensions).

## II. The Computational Model

The computational region in Hall 2De extends several channel lengths ( $L$ ) downstream of the thruster exit. A schematic of the physical domain with naming conventions for the various boundaries are provided in Figure 1. The typical extent of the computational region in an HPHall simulation is also shown for comparison. Ions are treated as an isothermal, cold (relative to the electrons) fluid, accounting for charge-exchange and multiple-ionization collisions in the momentum equations. Although electron-impact collisions that lead to the ionization of an atom can be frequent by comparison to its transit time inside the channel, for most Hall thrusters, collisions between the atomic species (“neutrals”) are rare. A popular numerical method for simulating the flow of neutrals in Hall thrusters is PIC combined with DSMC to account for ionization collisions. An inherent disadvantage of particle methods like PIC is the noise that is generated due to the particle statistics, which can be reduced by including more particles but at the expense of increased computation time. The method followed in Hall 2De is based on widely-used methods to model problems such as photon transport in radiation heat transfer problems<sup>6</sup> and is advancement over a previous algorithm that has been used to model regions of collisionless flows in electric propulsion hollow cathodes.<sup>23,24</sup> The method assumes that particles striking a surface are fully accommodated and that the fraction of those particles that is re-emitted follows a cosine distribution. The particle flux on any given surface depends then on the view factor between that surface and all other surfaces that emit particles. Because the basis for computing particle distributions in a region bounded by emission surfaces are the view factors the problem then becomes essentially a problem in geometry. The view factors can be computed at the pre-processing phase of the simulation thereby contributing an insignificant amount to the total computation time. The approach for the neutral gas is presented in a companion paper<sup>32</sup> and will not be described here. A 2-D form of Ohm’s law and the electron energy equation are solved for the electrons and the equations are discretized on a field-aligned computational mesh. Ohm’s law is combined with the current conservation equation to yield the plasma potential. The boundary conditions related to the sheath along the dielectric walls, and conditions for the remaining boundaries are provided in ensuing sections.

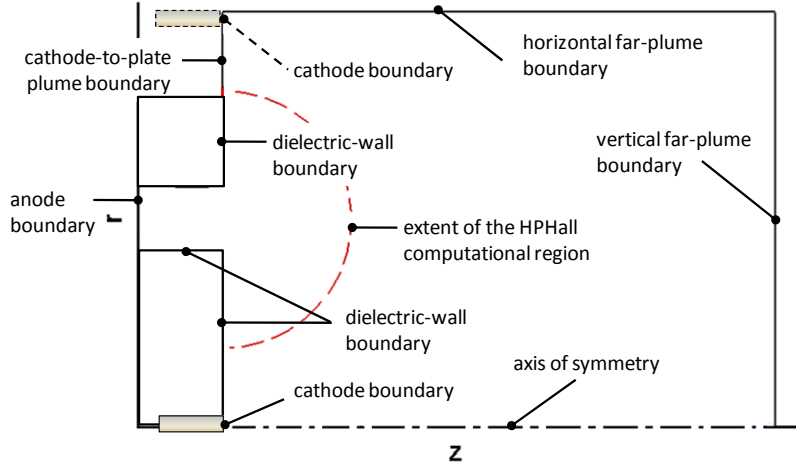


Figure 1. Schematic of the computational region and naming conventions for the boundary conditions.

### A. Ions

#### 1) Physics model

Because the treatment of ions, specifically the computational methods employed to determine their evolution inside the acceleration channel, has been wide-ranging due largely to the assumptions made on their characteristic collision scales, we outline our estimates of the relevant characteristic sizes for the ions in some detail. The two characteristic times for relaxation to a fluid,  $\tau_e$  for electrons and  $\tau_i$  for ions, are:

$$\begin{aligned}\tau_e &= \langle v_{ei} \rangle^{-1} = \frac{3(2\pi)^{3/2} \epsilon_0^2 \sqrt{m_e} (k_B T_e)^{3/2}}{n_i Z^2 e^4 \ln \Lambda} \\ \tau_i &= \langle v_{ii} \rangle^{-1} = \frac{12\pi^{3/2} \epsilon_0^2 \sqrt{m_i} (k_B T_i)^{3/2}}{n_i Z^4 e^4 \ln \Lambda} = \left( \frac{2m_i}{m_e} \right)^{1/2} \left( \frac{T_i}{T_e} \right)^{3/2} \frac{\tau_e}{Z^2}\end{aligned}\tag{II-1}$$

(with temperature expressed in K). Hereon, our convention will exclude the brackets from mean values of the collision frequency, that is  $v \equiv \langle v \rangle$ . For slow-moving ions the (Spitzer) thermal equilibration time between singly-charged ions and electrons when  $T_i \leq T_e$  may be approximated by

$$\tau_{ei}^T \approx \frac{m_i}{2m_e} \tau_e. \quad (\text{II-2})$$

Using estimated values in the 6 kW laboratory Hall thruster the ion transit time  $\tau_u = L/u_i$  can range approximately from  $(0.03 \text{ m})/(2 \times 10^4 \text{ m/s}) = 1.5 \text{ } \mu\text{s}$  for those ions that are accelerated downstream of the channel to  $(0.01 \text{ m})/(5 \times 10^2 \text{ m/s}) = 10 \text{ } \mu\text{s}$  for those generated near the anode region and lost to the walls. In comparison, the thermal equilibration time between electrons and ions ranges 0.03-0.5 s. inside the channel. This implies that the ions remain “cold” relative to the electrons. The (thermal) mean-free-path (mfp) for ion-ion collisions

$$\lambda_{ii} = u_{T,i} \tau_i, \quad (\text{II-3})$$

is plotted in Figure 2-left along the middle of the acceleration channel of the 6 kW Hall thruster for various (assumed) values of the ion temperature. The profiles have used the HPHall-computed values<sup>14</sup> for the plasma density and electron temperature. It will be shown later that the ion density may in fact be substantially higher in the anode region than the values predicted by HPHall, which suggests even smaller collision mfps for ions in this region than those plotted in Figure 2-left. Also, recent Laser-Induced Fluorescence measurements of  $\text{Xe}^+$  inside the 6 kW Hall thruster have shown that ions follow very closely the equilibrium distribution function,<sup>33</sup> which further strengthens the continuum assumption for the ions in this region. Figure 2-right depicts the charge-exchange collision mfp for ions with neutrals as estimated by,

$$\lambda_{in} = (\sigma_{in} n_n)^{-1}, \quad (\text{II-4})$$

and is plotted for two values of the charge-exchange cross section  $\sigma_{in}$ :  $50 \text{ } \text{\AA}^2$  and  $100 \text{ } \text{\AA}^2$ . Based on the measurements of Miller *et. al.*,<sup>34</sup> the two values cover the range of typical ion energies attained in the channel, <1 eV to 300 eV, with the higher value of the cross section representing the lowest energy ions. For comparison, the characteristic mfp for self collisions between neutrals

$$\lambda_{nn} = (\pi n_n D^2 \sqrt{2})^{-1}, \quad (\text{II-5})$$

is also plotted in Figure 1-right using a mean atomic diameter for xenon of  $D = 2.6 \text{ } \text{\AA}$ .<sup>35</sup>

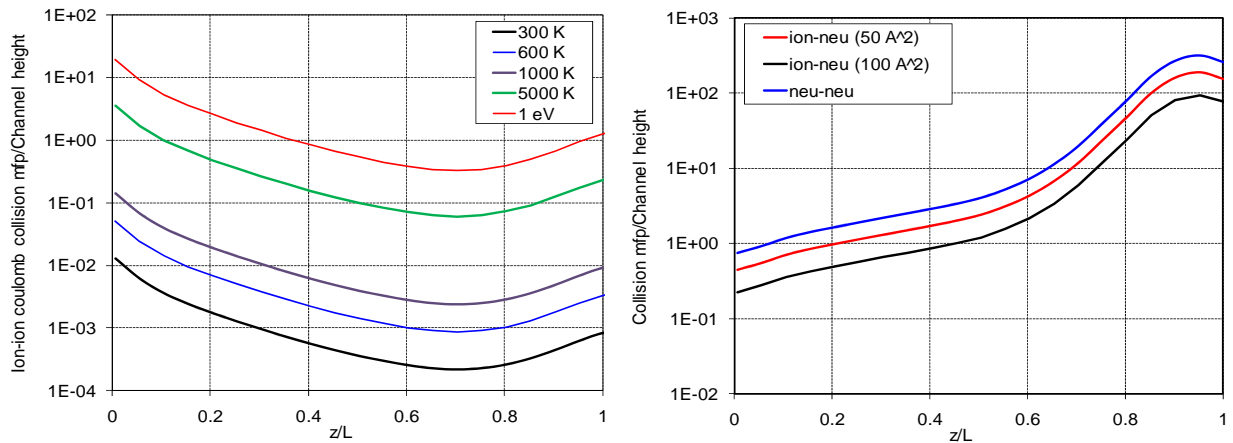


**Figure 2. Collisions mean free paths at the middle of the acceleration channel in the 6 kW laboratory Hall thruster. Left: Ion-ion coulomb collisions for different values of the ion temperature. Right: Ion-neutral collisions that lead to the exchange of charge and neutral-neutral collisions.**

Based on the estimates in Figure 2 the approach followed here is to treat ions as a fluid, and include charge-exchange collisions as a contribution to the (elastic) friction or “drag” force, whereas neutrals will be simulated using a collisionless approach.<sup>32</sup> It is noted that the addition of charge-exchange collisions can become increasingly important in the anode region since the electric force can be negligibly small there as by suggested by recent measurements of the plasma potential.<sup>36</sup>

The formulations that lead to the momentum conservation law begin with Boltzmann’s equation for the distribution function of ions  $f_i(t, \mathbf{r}, \mathbf{v})$

$$\frac{\partial f_i}{\partial t} + \mathbf{v} \cdot \nabla_{\mathbf{r}} f_i + \mathbf{F}_i \cdot \nabla_{\mathbf{v}} f_i = (\dot{f}_i)_c \quad (\text{II-6})$$

where  $\mathbf{F}_i$  is the total specific force (force/mass) on the ions containing the electric and Lorentz forces. The term on the right expresses the rate of change of the distribution function as a result of collisions between ions and species “s” and, in principle, it may be composed of both elastic and inelastic components. By taking the product of Eq. (II-6) with the ion momentum  $m_i \mathbf{v}_i$  and integrating over velocity space one obtains the conservation law for the transport of momentum:

$$\frac{\partial}{\partial t} (nm \langle \mathbf{v} \rangle)_i + \nabla_{\mathbf{r}} \cdot (nm \langle \mathbf{v} \mathbf{v} \rangle)_i - n_i m_i \langle (\mathbf{F} \cdot \nabla_{\mathbf{v}}) \mathbf{v} \rangle_i = \int m_i \mathbf{v} (\dot{f}_i)_c d\mathbf{v} \quad (\text{II-7})$$

Recall the definitions of the relevant velocities:  $\mathbf{v}$  is the particle velocity (with respect to the laboratory frame of reference),  $\mathbf{u} \equiv \langle \mathbf{v} \rangle = n^{-1} \int \mathbf{v} f d\mathbf{v}$  is the mean particle velocity and  $\mathbf{c} \equiv \mathbf{v} - \mathbf{u}$  is the particle thermal velocity. Hereinafter, the subscript from the spatial operator  $\nabla_{\mathbf{r}}$  shall be excluded. Accordingly, the various terms in Eq. (II-7) in the absence of the Lorentz force become

$$\begin{aligned} \frac{\partial}{\partial t} (nm \langle \mathbf{v} \rangle)_i &= \frac{\partial}{\partial t} (nm \mathbf{u})_i \\ \nabla \cdot (nm \langle \mathbf{v} \mathbf{v} \rangle)_i &= \nabla \cdot (nm \langle \mathbf{c} \mathbf{c} \rangle + nm \mathbf{u} \mathbf{u})_i \\ n_i m_i \langle (\mathbf{F} \cdot \nabla_{\mathbf{v}}) \mathbf{v} \rangle_i &= n_i q_i \mathbf{E} \\ \int m_i \mathbf{v} (\dot{f}_i)_c d\mathbf{v} &\equiv \mathbf{R}_i \end{aligned} \quad (\text{II-8})$$

The drag force density  $\mathbf{R}_i$ , defined in terms of the collision term on the right in Eq. (II-7), may be broken up into two parts to distinguish the momentum exchange between species by elastic collisions from that by inelastic collisions:

$$\mathbf{R}_i = \int m_i \mathbf{v} (\dot{f}_i)_c d\mathbf{v} \Big|_{\text{elastic}} + \int m_i \mathbf{v} (\dot{f}_i)_c d\mathbf{v} \Big|_{\text{inelastic}}. \quad (\text{II-9})$$

Because the dynamics of the direct and inverse elastic collisions are the same the term for collisions with species “s” may be approximated in terms of a mean collision frequency  $\nu$  between ions and other species “s”

$$\int m_i \mathbf{v} (\dot{f}_i)_c d\mathbf{v} \Big|_{\text{elastic}} \approx - \sum_{s \neq i} n_i m_i \nu_{is} (\mathbf{u}_i - \mathbf{u}_s). \quad (\text{II-10})$$

The momentum conservation law for ions may therefore be expressed in conservative form as follows:

$$\frac{\partial}{\partial t} (nm \mathbf{u})_i + \nabla \cdot (nm \mathbf{u} \mathbf{u})_i = q_i n_i \mathbf{E} - \nabla p_i + \mathbf{R}_i \quad (\text{II-11})$$

where we have neglected the viscous terms in the pressure tensor  $\mathbf{p}_i \equiv nm \langle \mathbf{c} \mathbf{c} \rangle$  and have assumed that  $\mathbf{p}_i = p_i \mathbf{I}$  (with  $\mathbf{I}$  being the unit or delta tensor). Equation (II-11) may be combined with the ion continuity

$$\frac{\partial(nm)_i}{\partial t} + \nabla \cdot (nm\langle \mathbf{v} \rangle)_i = \int m_i (\dot{f}_i)_c d\mathbf{v} = m_i \dot{n} \quad (\text{II-12})$$

to yield the momentum equation in non-conservative form

$$n_i m_i \left[ \frac{\partial \mathbf{u}_i}{\partial t} + (\mathbf{u}_i \cdot \nabla) \mathbf{u}_i \right] = q_i n_i \mathbf{E} - \nabla p_i + \mathbf{R}_i - \mathbf{u}_i m_i \dot{n} \quad (\text{II-13})$$

$$n_i m_i \frac{D\mathbf{u}_i}{Dt} \approx q_i n_i \mathbf{E} - \sum_{s \neq i} n_i m_i v_{is} (\mathbf{u}_i - \mathbf{u}_s) - \nabla p_i + \mathbf{S}_i$$

where  $\mathbf{S}_i$  includes all the inelastic contributions to the transport of ion momentum,

$$\mathbf{S}_i \equiv \int m_i \mathbf{v} (\dot{f}_i)_c d\mathbf{v} - m_i \mathbf{u}_i \dot{n}. \quad (\text{II-14})$$

It is noted that there are two terms in  $\mathbf{S}_i$  and they are mathematically distinct. The first appears as a direct consequence of taking the first moment of Eq. (II-6) to obtain the conservative form of the momentum equation (II-11). The second term appears because Eqs (II-11) and (II-12) were combined to obtain the non-conservative form of the momentum equation (II-13). For a quasi-neutral plasma with only singly-charged ions and no recombination,  $\mathbf{S}_i$  takes the simple form

$$\mathbf{S}_i = m_i \mathbf{u}_n \dot{n} - m_i \mathbf{u}_i \dot{n} = -m_i n_e v_{en}^I (\mathbf{u}_i - \mathbf{u}_n) \quad (\text{II-15})$$

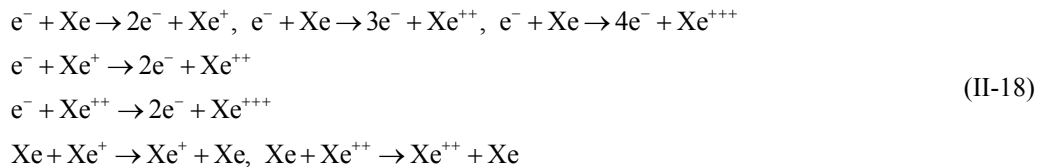
and, assuming only charge-exchange collisions for the elastic contributions in Eq. (II-10), Eq. (II-13) is simplified as follows:

$$n_i m_i \frac{D\mathbf{u}_i}{Dt} = q_i n_i \mathbf{E} - \nabla p_i - n_i m_i (v_{in} + v_{en}^I) (\mathbf{u}_i - \mathbf{u}_n) \quad (\text{II-16})$$

to yield the ion velocity field. Multiply-charged ions may be accounted for by following the same formulations outlined above while including the relevant ionization collision frequencies for the higher charge states. The last term on the right of Eq. (II-16) may in fact be expressed more generally in terms of an “ion generation rate” that includes both charge-exchange and electron impact-ionization collisions as follows:

$$-m \sum_{i' < i} \dot{n}_{i' \rightarrow i} (\mathbf{u}_i - \mathbf{u}_{i'}) \quad (\text{II-17})$$

with  $i' \rightarrow i$  denoting the direction of the reaction. For example, for collisions that generate singly-charged ions from neutrals,  $\text{Xe} \rightarrow \text{Xe}^+$ , then  $i'=0$  and  $i=1$  and so forth and so on. In the present model we account for the following reactions listed in Eq. (II-18) with all collision cross sections specified based on available data. The drag between multiply-charged ions  $\sim n_i^Z m_i v_{ii}^Z (\mathbf{u}_i^Z - \mathbf{u}_i^{Z+1})$  has not yet been included in Eq. (II-16).



For the results presented in this paper a constant temperature of 500 °C has been assumed for the ions. Although no sensitivity calculations have been performed yet to assess the impact of the assumption on the solution, it is not expected to have a significant effect since the ion temperature affects only the ion pressure and the ion-neutral

collision frequencies. On-average the latter has a square-root dependence on the temperature and the ion-pressure gradient force is negligible compared to the other forces; this will be further quantified in an ensuing section. Also, in the case of the heavy species with different masses,  $m$  in expression (II-17) would be proportional to the reduced mass,  $m_i m_r / (m_i + m_r)$ , but since here only xenon ions and atoms are present  $m$  denotes the mass of the heavy species.

The system of conservation laws for the ions is closed with conditions specified at all boundaries in Figure 1. At the anode and dielectric-wall boundaries the Bohm condition is prescribed for the speed with which the ions exit the physical domain (i.e. at entry to the sheath). At the plume boundaries the ions are allowed to flow out of the system freely (gradients of the two velocity components are set to zero). Reflection boundary conditions are set at the axis of symmetry. Presently no ion flux is specified to flow from the cathode boundary into the physical domain.

## 2) Numerical approach

Equation (II-16) is solved using a first-order upwind scheme for the velocity field at the vertices,  $\mathbf{u}_{\text{ver}}$ . Since the simulation domain is comprised of quadrilateral computational cells of arbitrary shape as shown in Figure 3-left the scheme accounts for the surrounding eight vertices (open circles) to determine the upwind direction. Because all the conservation laws in Hall 2De are discretized using finite-volume differencing, scalars (such as the number density  $n_{\text{cel}}$ ) are computed at the cell centers and vectors (such as forces  $\mathbf{F}_{\text{edg}}$  and fluxes) are computed at the cell edges. The ion momentum equation is the only conservation law solved in non-conservative fashion so it requires that both vectors and scalars be known at vertices. Referring to Figure 3-middle and -right, the algorithm uses bilinear interpolation at each vertex for edge-centered (middle) and cell-centered quantities (right) using the quadrilateral defined by the dashed lines. Equations (II-12) and (II-16) are marched explicitly from time  $t$  to yield new values for the ion density and velocity field at  $t+\Delta t$ .

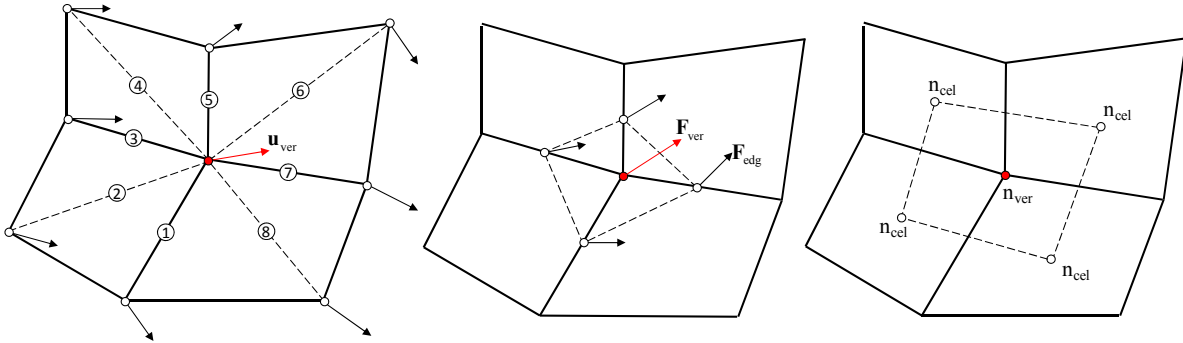


**Figure 3. Left: The ion momentum equation is solved in non-conservative form for the velocity field at the vertices using a first-order upwind scheme that takes into account the contributions from a maximum of eight surrounding vertices. Middle: Bilinear interpolation is used to define forces at vertices using their primitive values at the cell edges. Right: Bilinear interpolation is used to define scalar quantities at vertices using their primitive values at the cell centers.**

## A. Electrons

### 1) Physics model

The electron momentum equation in the absence of the viscous terms and assuming  $\mathbf{p}_e = p_e \mathbf{I}$  is given in vector form by:

$$n_e m_e \frac{D\mathbf{u}_e}{Dt} = -en_e (\mathbf{E} + \mathbf{u}_e \times \mathbf{B}) - \nabla p_e + \mathbf{R}_e \quad (\text{II-19})$$

As in the case for ions, the friction force  $\mathbf{R}_e/n_e$  for electrons is related to the integral of the collision term in the electron distribution function and the electron momentum. For the case of a near (or “quasi”)–Maxwellian distribution function in an anisotropic, classical plasma (i.e. with no random fluctuations in the fields)  $\mathbf{R}_e$  may be approximated as follows, assuming  $\mathbf{u}_e \gg \mathbf{u}_n$ :

$$\mathbf{R}_e \approx -n_e m_e \left[ \sum_i v_{ei} (\mathbf{u}_e - \mathbf{u}_i) + v_{en} \mathbf{u}_e \right] = e^{-1} m_e (\bar{v}_{ei} + v_{en}) \mathbf{j}_e + (eZ^*)^{-1} m_e \bar{v}_{ei} \sum_i Z_i \mathbf{j}_i \quad (\text{II-20})$$



with the electron and ion current densities defined as  $\mathbf{j}_e = -en_e \mathbf{u}_e$  and  $\mathbf{j}_i = q_i n_i \mathbf{u}_i = eZn_i \mathbf{u}_i$  respectively, and the total electron-ion (e-i) collision frequency given by

$$\bar{\nu}_{ei} = \frac{n_e Z^* e^4 \ln \Lambda}{3(2\pi)^{3/2} \epsilon_0^2 \sqrt{m_e} (k_B T_e)^{3/2}} \quad Z^* \equiv n_e^{-1} \sum_i n_i Z^2. \quad (\text{II-21})$$

Unless otherwise noted all references to “e-i collision frequency” in the remainder of this paper shall imply the definition in Eq. (II-21). If the electron inertia can be neglected then one obtains the vector form of Ohm’s law

$$\mathbf{E} = \eta_0 \mathbf{j}_e + \eta_0 \Omega_0 \mathbf{j}_e \times \hat{\boldsymbol{\beta}} - \frac{\nabla p_e}{en_e} + \eta_{ei} \bar{\mathbf{j}}_i \quad (\text{II-22})$$

where

$$\eta_0 = \frac{m_e (\bar{\nu}_{ei} + \nu_{en})}{e^2 n_e} \quad \eta_{ei} = \frac{m_e \bar{\nu}_{ei}}{e^2 n_e} \quad \hat{\boldsymbol{\beta}} = \mathbf{B}/B \quad \Omega_0 = \frac{|B|}{en_e \eta_0} \quad \bar{\mathbf{j}}_i = \frac{1}{Z^*} \sum_i Z \mathbf{j}_i. \quad (\text{II-23})$$

In the frame of reference of the magnetic induction field with “//” and “ $\perp$ ” denoting parallel and perpendicular components respectively, the components of Eq. (II-22) may be written as

$$E_{//} = \eta_0 j_{e//} - \frac{\nabla_{//} p_e}{en_e} + \eta_{ei} \bar{j}_{i//} \quad E_{\perp} = \eta_0 (1 + \Omega_0^2) j_{e\perp} - \frac{\nabla_{\perp} p_e}{en_e} + \eta_{ei} \bar{j}_{i\perp}. \quad (\text{II-24})$$

It is noted that in the absence of the ion velocity in the electron drag force density (Eq. (II-20)), Eqs (II-24) take a form that is suitable for problems involving electron diffusion in weakly-ionized plasmas

$$\mathbf{j}_{e//} = en_e \mu_0 \left( E_{//} + \frac{\nabla_{//} p_e}{en_e} \right) \quad \mathbf{j}_{e\perp} = \frac{en_e \mu_0}{1 + \Omega_0^2} \left( E_{\perp} + \frac{\nabla_{\perp} p_e}{en_e} \right) \quad (\text{II-25})$$

The form of Ohm’s law given in Eq. (II-25), using the electron mobility  $\mu_0$  instead of the resistivity (note  $\mu_0 = 1/en_e \eta_0$ ), is the form that has traditionally been implemented in Hall thruster models such as HPHall.<sup>7</sup> Equations (II-25) imply the approximation  $\mathbf{u}_e \gg \mathbf{u}_i$  (in addition to  $\mathbf{u}_e \gg \mathbf{u}_n$ ) and thus  $\mathbf{R}_e \approx -n_e m_e \nu_0 \mathbf{u}_e$  with the total collision frequency “ $\nu_0$ ” representing the contributions from classical collisions of electrons with all other species. It has also been suggested that the diffusion of electrons in Hall thrusters is enhanced in a non-classical manner, e.g. by plasma turbulence, and attempts to capture this enhancement in numerical simulations with HPHall have been made through the use of an effective collision frequency<sup>7</sup> based on Bohm’s 1/B scaling for the cross-field mobility.<sup>10</sup> That is,  $\mathbf{R}_e \approx -n_e m_e (\nu_0 + \nu_B) \mathbf{u}_e$  where,

$$\nu_B = \frac{\alpha}{16} \omega_{ce} \quad (\text{II-26})$$

with  $\alpha$  being a constant. During their azimuthal drift electrons may also collide with walls and this has been proposed (originally by Morozov<sup>21</sup>) to be one more process that affects the transport of electrons in the acceleration channel. In numerical simulations of Hall thrusters this additional transport mechanism has been accounted for through the addition of another effective collision frequency  $\nu_{ew}$ . Because this frequency is found to be important only in regions where the quasi-1D assumption is valid the approach used to determine it is the same as that used in HPHall.<sup>13</sup> Accounting for all transport mechanisms effective values of the electrical resistivity and the Hall parameter may be defined as follows:

$$\eta \equiv \frac{m_e (\bar{\nu}_{ei} + \nu_{en} + \nu_{ew} + \nu_B)}{e^2 n_e} \quad \Omega_e \equiv \frac{|B|}{en_e \eta}. \quad (\text{II-27})$$

Unless otherwise noted, all references to the “Hall parameter” in the remainder of this paper shall imply the definition in Eq. (II-27). In Section III a series of numerical simulations will be presented that compare results obtained by Hall 2De with those obtained recently by HPHall for two Hall thrusters, the BPT-4000 and the 6 kW Hall thruster.<sup>13,14</sup> In these simulations the HPHall solutions incorporate a spatially varying  $\alpha$  that is guided by plasma measurements and by the observed operational characteristics of the thrusters (such as discharge current and thrust). The presence of turbulence, its real effect on electron transport and the question of whether it can be quantified using Bohm’s formula has been an ongoing area of research. As a consequence, in models like HPHall the variation of  $\alpha$  from one thruster simulation to another is not based on first principles, which presents the biggest obstacle in advancing such models to fully-predictive design tools for Hall thrusters.

The overall system of conservation laws is augmented with an equation for the conservation of current

$$\nabla \cdot (\mathbf{j}_e + \mathbf{j}_i) = 0 \quad (\text{II-28})$$

and the equation for the electron temperature (expressed in eV)

$$\frac{3}{2} n_e \frac{\partial T_e}{\partial t} = \mathbf{E} \cdot \mathbf{j}_e + \nabla \cdot \left( \frac{5}{2} T_e \mathbf{j}_e + \boldsymbol{\kappa}_e \cdot \nabla T_e \right) - \frac{3}{2} T_e \nabla \cdot \mathbf{j}_e - \sum_s \dot{n}_s e \left( \epsilon_s + \frac{3}{2} T_e \right) + Q_e^T. \quad (\text{II-29})$$

The last term on the right represents the energy exchange per unit time between electrons and the heavy species<sup>37</sup> due to deviations from thermal equilibrium and is proportional to  $n_e(m_e/m)v_{ei}(T_e - T_i)$  for ions and  $n_e(m_e/m)v_{en}(T_e - T_n)$  for neutrals. In Hall thrusters it is usually a small contribution to the total electron energy content.

The equations for the electrons are closed with boundary conditions at all surfaces in Figure 1. As it will be shown in the next subsection, Eq. (II-28) is in fact combined with Eq. (II-24) to yield the plasma potential, and requires boundary conditions either for the plasma potential, its gradient or for the current density. For all dielectric-wall boundaries a zero-current condition is imposed,  $\mathbf{j}_e = \mathbf{j}_i$ . At the anode a Dirichlet condition specifies directly the voltage at its discharge value. For both simulation cases that are presented in this paper this value is 300 V. A Dirichlet condition is also imposed at the cathode with a value of 0 V. For the electron energy the convective heat loss follows the formulations of Hobbs and Wesson (H&W)<sup>38</sup> using a fit<sup>39</sup> for the H&W solution of the sheath potential as a function of the secondary electron yield (SEE). The Maxwellian-averaged SEE is also specified using a fit to data for the dielectric material used in each thruster. A Dirichlet condition for the electron temperature is also imposed at the anode.

## 2) Numerical approach

The large disparity ( $>2$  orders of magnitude in regions with high values of the magnetic field) that exists in the electron transport equations in the perpendicular versus the parallel directions requires special treatment. One approach is to solve the equations for electrons only in the perpendicular direction; this quasi-1D approach is followed by HPHall and other similar models of Hall thrusters. This evades the numerical difficulties associated with the resolution of transport in both directions and is an excellent approximation for most of the acceleration channel and near-plume regions. To extend the solution to regions in the far plume and/or to resolve regions of the magnetic field with complex topology requires a 2-D solution of the electron transport equations. To accomplish this, the approach followed here is to solve the equations in the frame of reference of the magnetic field, in two dimensions ( $\hat{\boldsymbol{\beta}} = \beta_r \hat{\mathbf{r}} + \beta_z \hat{\mathbf{z}}$ ). To diminish excessive numerical diffusion all equations are discretized in a computational mesh that is aligned with the magnetic field. In this section the general approach is outlined using Eq. (II-28) as the example equation.

The plasma potential in Hall 2De is solved by combining the equation for current conservation and Ohm’s law into one equation. Then for a single quadrilateral computational cell with volume  $\Delta V$  the divergence theorem allows for the following discretization:

$$\begin{aligned} \nabla \cdot \mathbf{j}^{t+\Delta t} \Delta V &= \sum_{\text{edg}=1}^4 (\mathbf{j}^{t+\Delta t} \cdot \hat{\mathbf{n}} \Delta A)_{\text{edg}} \\ &= \sum_{\text{edg}=1}^4 \left\{ \left[ (\mathbf{j}^{t+\Delta t} \cdot \hat{\boldsymbol{\beta}}) \hat{\boldsymbol{\beta}} - \hat{\boldsymbol{\beta}} \times (\hat{\boldsymbol{\beta}} \times \mathbf{j})^{t+\Delta t} \right] \cdot \hat{\mathbf{n}} \Delta A \right\}_{\text{edg}} \end{aligned} \quad (\text{II-30})$$

The dot product in Eq. (II-30) at a edge may be expanded as

$$\left[ (\mathbf{j}^{t+\Delta t} \cdot \hat{\boldsymbol{\beta}}) \hat{\boldsymbol{\beta}} - \hat{\boldsymbol{\beta}} \times (\hat{\boldsymbol{\beta}} \times \mathbf{j}^{t+\Delta t}) \right] \cdot \hat{\mathbf{n}} \approx \eta^{-1} (\mathbf{E}^{t+\Delta t} + \boldsymbol{\varepsilon}^t) \cdot \bar{\mathbf{n}}^t \quad (\text{II-31})$$

where

$$\begin{aligned} \bar{\mathbf{n}} &\equiv \bar{\mathbf{n}}_r + \bar{\mathbf{n}}_z \\ \bar{\mathbf{n}}_r &= \beta_r (\beta_r \hat{\mathbf{r}} + \beta_z \hat{\mathbf{z}}) \cdot \hat{\mathbf{n}} + \frac{\beta_z}{1 + \Omega_e^2} (\beta_z \hat{\mathbf{r}} - \beta_r \hat{\mathbf{z}}) \cdot \hat{\mathbf{n}} \\ \bar{\mathbf{n}}_z &= \beta_z (\beta_r \hat{\mathbf{r}} + \beta_z \hat{\mathbf{z}}) \cdot \hat{\mathbf{n}} - \frac{\beta_r}{1 + \Omega_e^2} (\beta_z \hat{\mathbf{r}} - \beta_r \hat{\mathbf{z}}) \cdot \hat{\mathbf{n}} \end{aligned} \quad (\text{II-32})$$

and  $\mathbf{E} = -\nabla\phi$ . The remaining terms in Eq. (II-24) involving the electron pressure and the ion current terms are included in the term “ $\boldsymbol{\varepsilon}$ .” Equation (II-30) is solved implicitly for the plasma potential. It is noted that a simplification occurs in Eqs (II-32) when the computational mesh is aligned with the magnetic field, as illustrated in Figure 4. Numerical diffusion due to the disparity between the terms with and without  $\Omega_e$  is reduced by assuming that cell edges are exactly either parallel or perpendicular to the magnetic field lines. The accuracy of the solution is then dependent upon the extent of the spatial deviations of the mesh from the true lines of constant potential and stream functions  $\chi$  and  $\psi$ . Here,  $\chi$  and  $\psi$  are the commonly-used set of conjugate harmonic functions satisfying the Cauchy-Riemann conditions for the radial and axial components of the magnetic field.

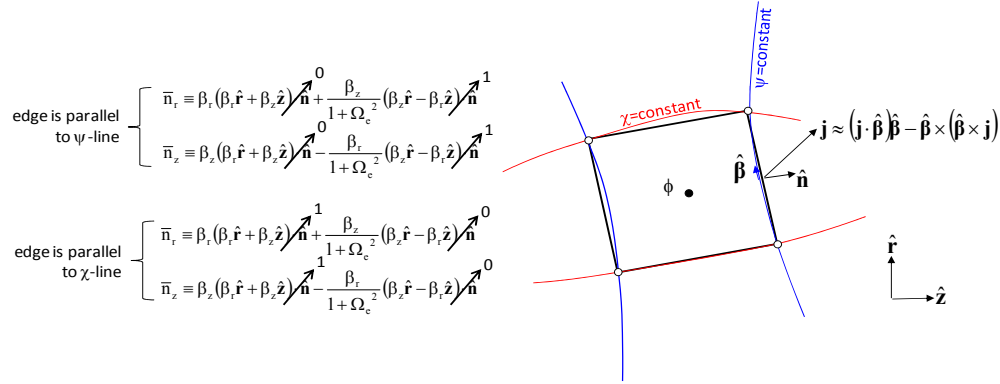


**Figure 4. Each edge of a computational cell in Hall 2De is closely aligned with either a line of constant potential function ( $\chi$ ) or a line of constant stream function ( $\psi$ ).**

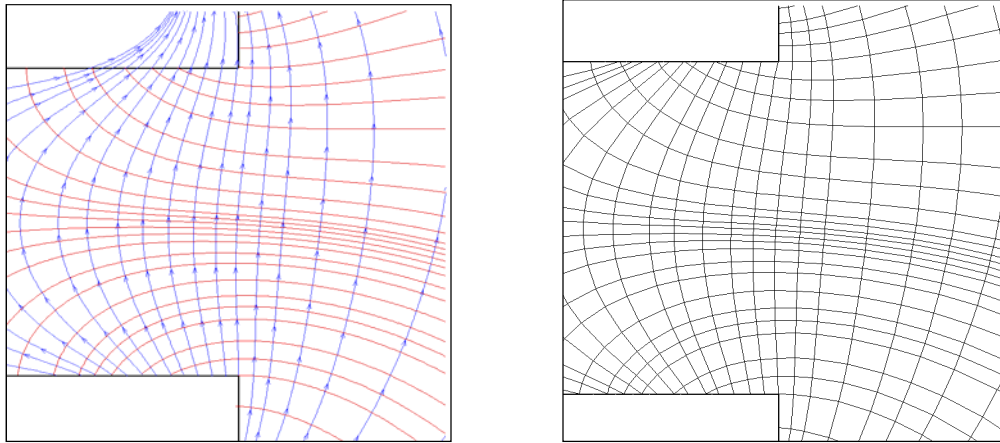


**Figure 5. Left: A set of lines of constant stream function ( $\psi$ ) in blue (streamlines of the magnetic field) overlaid by lines of constant potential function ( $\chi$ ) in red, in the vicinity of the acceleration channel in the 6 kW Hall thruster. Right: corresponding finite-element computational mesh.**

The computational mesh is generated first by superimposing lines of constant  $\chi$  and  $\psi$  onto the computational region using commercially available graphics software (Figure 5-left). The computational region boundaries are specified by line segments that connect points used to specify the geometry of the region. Then the spatial locations of points along each line, generated by integration in space along each streamline, are extracted. Each pair of adjacent points along a  $\chi$ -line (or a  $\psi$ -line) defines a line segment. A mesh algorithm then searches for the intersections between all line segments over all  $\chi$ -lines,  $\psi$ -lines and boundary lines. Each intersection defines a vertex location and these vertices are then used to generate the finite element mesh shown in Figure 5-right. The equation for the electron temperature is solved in a semi-implicit fashion. The thermal conduction term is implicit whereas all other terms are evaluated at the previous time-step as expressed by Eq. (II-33).

$$\frac{3}{2} n_e^t \frac{T_e^{t+\Delta t} - T_e^t}{\Delta t} - \nabla \cdot (\kappa_e^t \cdot \nabla T_e^{t+\Delta t}) \approx \left[ \mathbf{E} \cdot \mathbf{j}_e + \nabla \cdot \left( \frac{5}{2} T_e \mathbf{j}_e \right) - \frac{3}{2} T_e \nabla \cdot \mathbf{j}_e - \sum_s \dot{n}_s e \left( \varepsilon_s + \frac{3}{2} T_e \right) + Q_e^T \right]^t \quad (\text{II-33})$$

### III. Numerical Simulations

#### A. Benchmark simulations with the BPT-4000

As a first series of Hall 2De algorithm tests we performed comparisons with existing numerical simulation results<sup>13</sup> obtained by HPHall for the BPT-4000 operating at 4.5 kW. The operational characteristics of this thruster as used in the numerical simulations are outlined in Table 1. The simulations employed the same spatial variations of the Bohm collision frequency factor  $\alpha$  in the acceleration channel and near-plume regions as in the HPHall simulations. It is noted that in those simulations the factor was significantly lower inside the acceleration channel ( $\alpha=0.035$ ) compared to the plume region ( $\alpha=1.0$ ). Moreover, beyond the effective HPHall computational region, defined by a near-anode magnetic-field streamline and a near-cathode streamline (as defined by the two streamlines in black in Figure 6) both the Bohm collision frequency and the Hall parameter are set to zero. For this first series of algorithm tests the spatial variations for  $v_B$  and  $\Omega_e$  in Hall 2De is the same as in HPHall but with a slightly more gradual reduction to zero (using a Gaussian function) downstream of the cathode field line. The one-on-one comparisons along a line that crosses the middle of the acceleration channel are shown in Figure 7. The benchmark simulations have also used the same model for the wall collision frequency  $v_{ew}$ .

The comparisons in Figure 7 and the 2-D contour plots in Figure 8 show similar solutions but with some marked differences. The overall heating of electrons appears to be in close agreement between the two solutions, which is expected since the peak electron temperature and its spatial variation near this maximum is driven mainly by resistive heating that is dominated by the Bohm collision frequency. By comparison to the other collision frequencies,  $v_B$  is at least one order of magnitude higher at the exit and near-plume regions where the maximum in the temperature is computed. Near the anode the electron temperature in Hall 2De is determined largely by the anode Dirichlet boundary condition (currently specified as 1 eV) and the surrounding dielectric-wall conditions, which prescribe the same H&W solution<sup>38</sup> as in HPHall for the convective heat loss of electrons in the sheath.

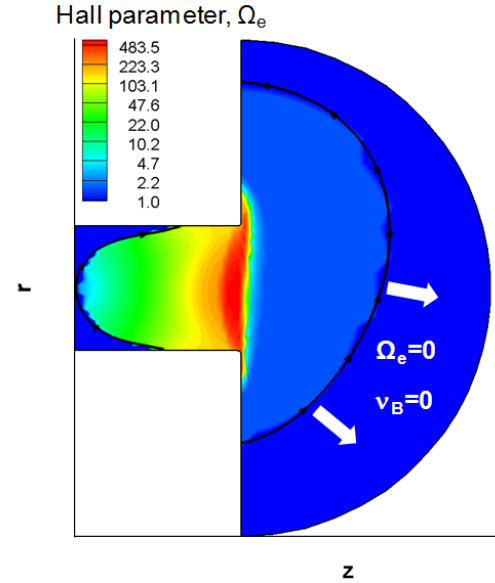


**Figure 6. Contours of the Hall parameter as computed by HPHall in the 6 kW Hall thruster simulations.<sup>14</sup> Near-anode and near-cathode streamlines define the effective HPHall computational domain beyond which  $\Omega_e$  and  $v_B$  are set to zero. The same approach is followed in the BPT-4000 simulations.<sup>13</sup>**

**Table 1. Operational characteristics used in the numerical simulations of the BPT-4000 at 4.5 kW.**

Thruster parameter	Value
Discharge (or anode) current (A)	15
Discharge voltage (V)	300
Anode mass flow rate (mg/s)	15.5
Cathode mass flow rate (mg/s)	1.55

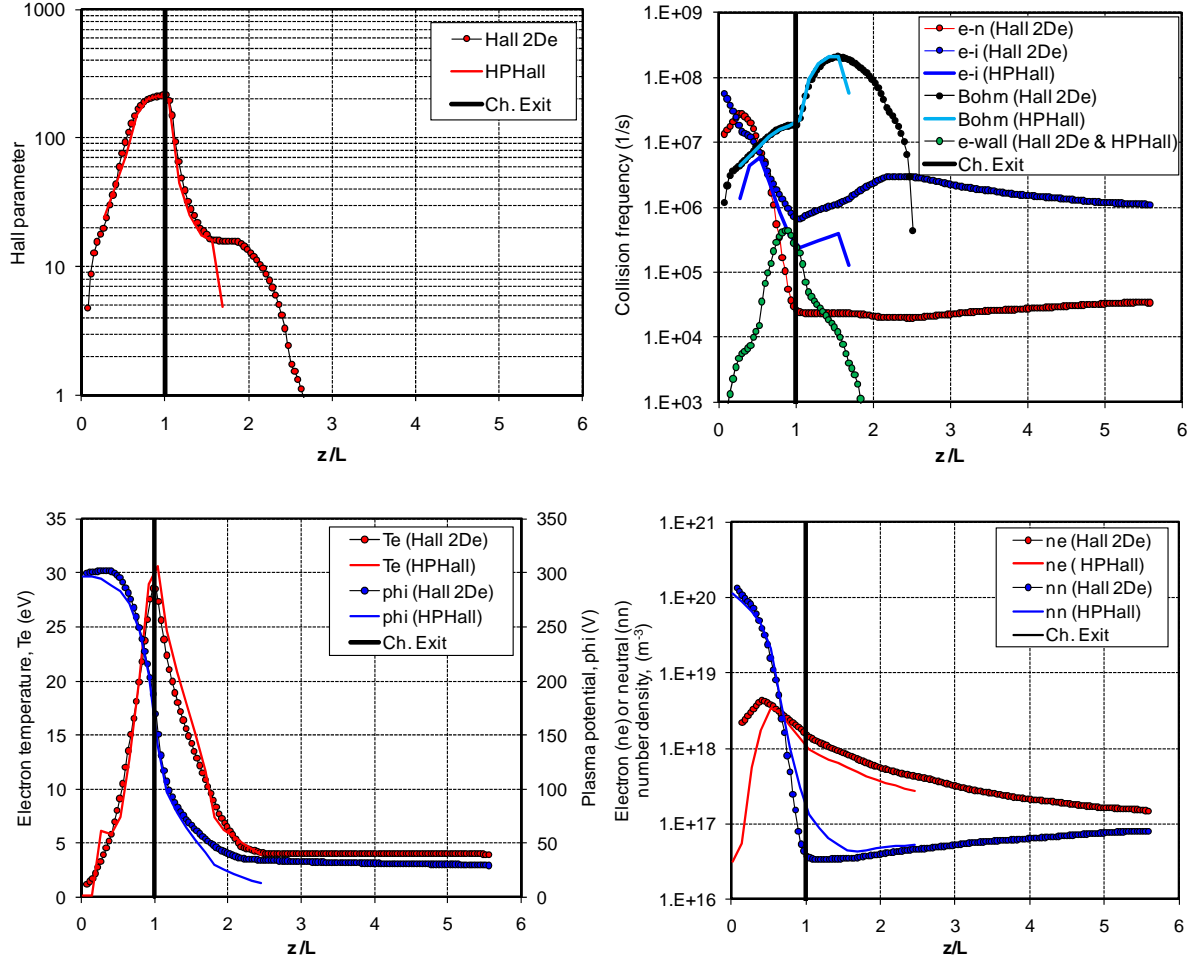


**Figure 7. Axial slice plots from the benchmark numerical simulations of the BPT-4000. The plots compare the solution obtained by HPHall<sup>13</sup> with that obtained by Hall 2De at the middle of the acceleration channel. In these benchmark simulations the Hall 2De simulations enforce a reduction of the Bohm collision frequency and of the Hall parameter beyond  $z/L \sim 1.5$  to emulate the approach followed in the HPHall simulations.**

A notable distinction between the solutions for the electron number density and plasma potential is evident in the anode region. This is illustrated in Figure 7 (bottom), Figure 8 (top), and is more evident in the axial profiles of Figure 9 (left). Hall 2De computes a higher plasma density in this region with values for  $z/L < 0.2$  exceeding one order of magnitude those obtained by HPHall. A comparison of the terms in Eq. (III-1) show that the anode region is dominated by ion diffusion since this is where the electric field is negligible. It is noted that as part of the inherent assumptions associated with the PIC simulation of ions the ion drag terms (numbered as “IV” in Eq. (III-1)) are not accounted for in HPHall. The ion pressure is also excluded in HPHall and the Hall 2De simulations confirm this to be a good approximation for the assumed ion temperature. The comparison of all the ion momentum terms in steady

state is shown in Figure 9-right. The effect of mesh resolution on the solution has not yet been quantified but, if of any significance, this is expected to influence the solution only in the very-near anode regions where the mesh is coarsest.

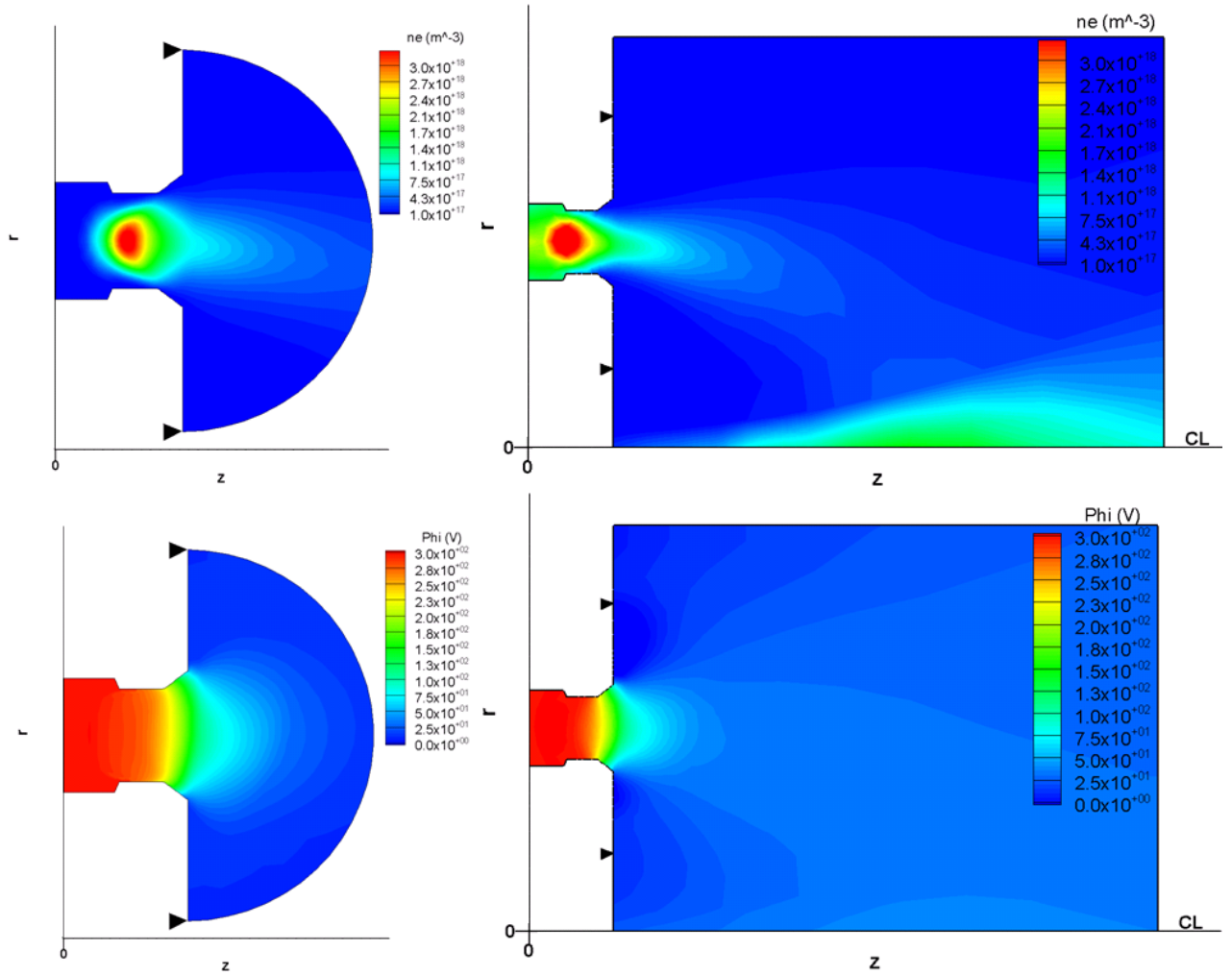


**Figure 8. Contour plots from the numerical simulations of the BPT-4000. The plots compare the 2-D solution<sup>13</sup> obtained by HPHall (left) with that obtained by Hall 2De (right). For these benchmark simulations Hall 2De and HPHall use approximately the same model for the spatial variation of the Bohm collision frequency. The arrows point to the maximum radial extent of the HPHall computational region. Top: electron number density. Bottom: plasma potential.**

$$\frac{\partial \mathbf{u}_i}{\partial t} \approx \frac{q_i}{m_i} \mathbf{E} + (-\mathbf{u}_i \cdot \nabla) \mathbf{u}_i + \frac{-\nabla p_i}{n_i m_i} + (v_{in} + v_{en}^I) (\mathbf{u}_n - \mathbf{u}_i) \quad (\text{III-1})$$

(I)
(II)
(III)
(IV)

A related effect is associated with the variation of the electric field in this region where measurements<sup>40</sup> have suggested little to no variation of the plasma potential (i.e.  $E_z \approx 0$ ). Similar comparisons as those performed for the ion momentum may be carried out for the dominant terms in Ohm's law, namely the resistive term and the electron pressure. These comparisons suggest that the higher plasma density reduces significantly the importance of these terms in this region such that any differences between them (the numerator in Eq. (III-2)), that would otherwise generate a finite electric field, are reduced. The numerator in Eq. (III-2) is reduced further by comparison to the HPHall solution since the total classical collision frequency is higher (first term) and the density gradient is lower

(second term). The e-i collision frequency is found to be higher in the near-plume regions as well, in part due to the higher plasma density there but largely as a result of accounting for the multiply-charged ions in Eq. (II-21) (through  $Z^*$ ); more notable however in the Hall 2De results is its continued rise downstream of the HPHall computational region. This rise is largely due to the colder electron temperature since the frequency is proportional to  $T_e^{-3/2}$ .

$$E_{\perp} \approx \eta_0 (1 + \Omega_e^2) j_{e,\perp} - \frac{\nabla_{\perp} p_e}{en_e} \sim \frac{j_{e,\perp} B^2 / m_e (v_{ei} + v_{en}) - T_e \nabla_{\perp} n_e}{n_e} \quad (\text{III-2})$$

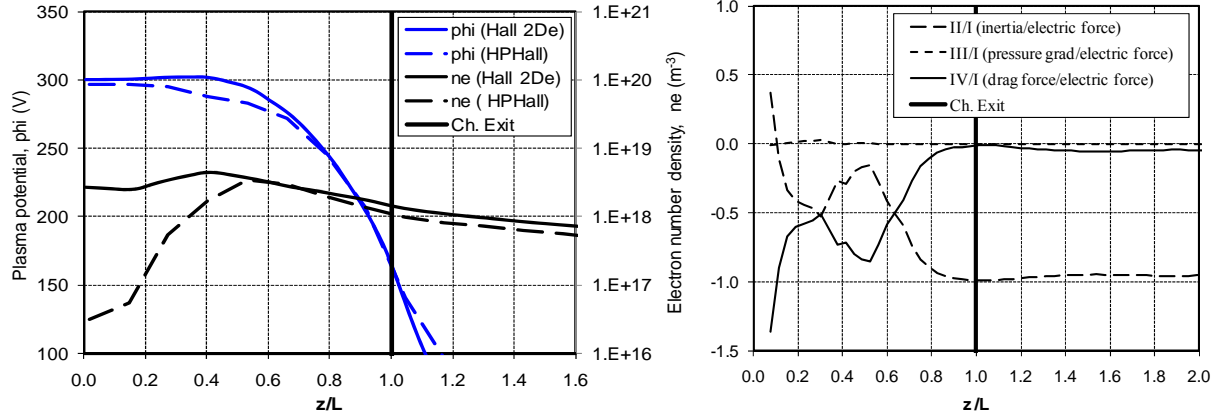


**Figure 9. Comparison of terms in the ion momentum conservation law for singly charged ions (Eq. (III-1)) along the mid-channel line of the BPT-4000 for the steady-state benchmark simulation case. The profiles on the right identify the anode or “ion-diffusion” region ( $z/L < 0.3$ ), the ionization region ( $0.3 < z/L < 0.6$ ) and the ion-acceleration region ( $z/L > 0.6$ ).**

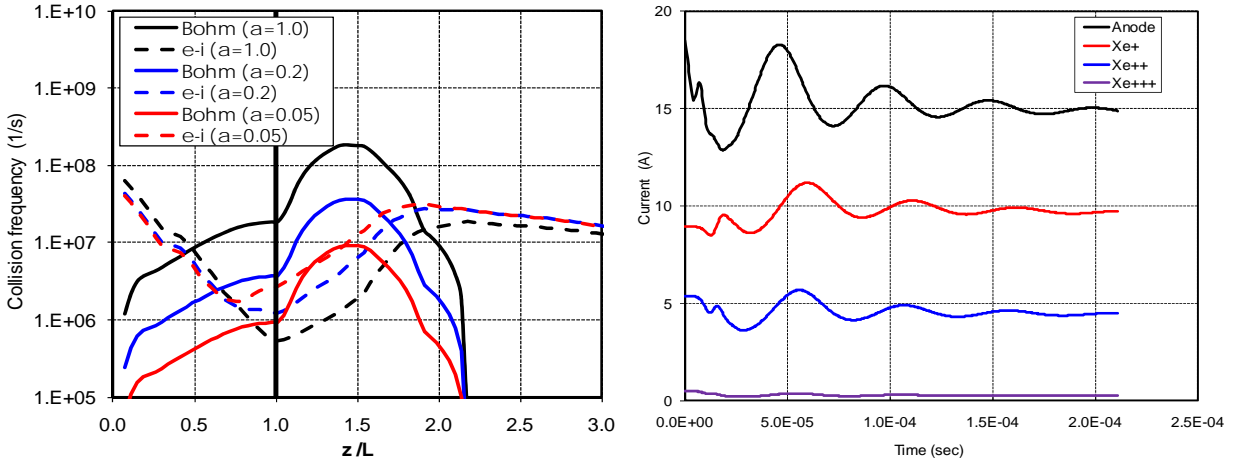
The capacity to resolve this rise due to Hall 2De’s extended computational region prompted a series of preliminary simulations to better understand the response of the plasma, specifically that of the e-i collision frequency, since it dominates over both the electron-neutral (e-n) and the electron-wall (e-w) frequencies beyond the ionization region. Figure 10-left shows the computed e-i collision frequency for three different values of the maximum Bohm factor:  $\alpha=1.0$ ,  $0.2$  and  $0.05$ . It should be clarified that we use “maximum” here because, as also noted earlier,  $\alpha$  is varied in the physical domain: for the BPT-4000 benchmark simulations in Figure 7,  $\alpha(=\alpha_c$  in Ref. 13) $=0.035$  inside the channel,  $\alpha(=\alpha_p$  in Ref. 13) $=1.0$  in the near-plume and for  $z/L > \sim 1.5$   $\alpha_p$  is reduced to zero. So, when we decrease the Bohm factor in this paper to, say,  $\alpha=0.2$  we imply a global reduction of the Bohm collision frequency, that is  $v_B=(0.035 \times 0.2)\omega_{ce}/16=0.007\omega_{ce}/16$  inside the channel and  $v_B=(1.0 \times 0.2)\omega_{ce}/16=0.2\omega_{ce}/16$  in the near-plume.

The results in Figure 10-left show an increasing e-i collision frequency with decreasing  $\alpha$  mainly because of the reduced electron temperature in the near-plume. The plasma density is also found to be higher than the HPHall values along the mid-channel line. The computed profiles for the electron temperature are shown in Figure 11. The anode current (15 A) is obtained for a maximum  $\alpha \approx 0.2$ , an  $\sim 80\%$  lower value than that used in the Hall 2De-HPHall benchmark simulations. For this spatial variation and value of maximum  $\alpha$  the ion (beam) current is found to  $I_b=(I^+)+(I^{++})+(I^{+++})=9.7+4.5+0.3=14.5$  A. Also, the solution for the anode and beam currents in Figure 10-right exhibits a periodic character but one that is under-damped; all current oscillations die out within a few periods. The damping of the oscillations occurs faster (within approximately one period) for  $\alpha=1.0$  and produces  $\sim 3.5$  A more current to the anode than the nominal value. The case of  $\alpha=0.05$  produces current oscillations that do not die out albeit at 1.2 A lower time-averaged anode current. We recall that  $v_B$  does not depend on any plasma parameters that could participate in and/or induce plasma oscillations, and we postulate this to be the reason for the damping of the oscillations when  $v_B$  is the dominant collision frequency. Low-frequency oscillations in the Hall 2De solution at low values of  $\alpha$  are also obtained in the 6 kW Hall thruster simulations to be presented in the next subsection.

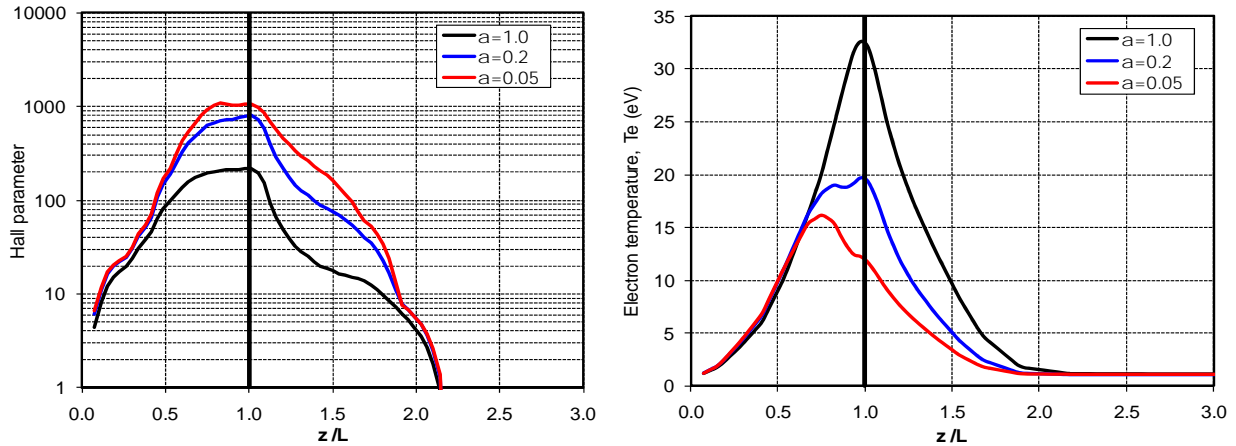
The increase of the e-i collision frequency to values that are comparable to or higher than the Bohm collision frequency is of significance in part because, to the best of our knowledge, the transport of electrons from regions of the plume that extend beyond the HPHall physical domain has not yet been resolved. In view of these elevated values of the e-i collision frequency in the far-plume, we attempt in the next section to lift the reduction of the Hall



parameter and Bohm collision frequency that was imposed as part of the BPT-4000 benchmark simulations. In recognition of the sensitivity of the e-i collision frequency on the electron temperature, we end this section with a calculation that assesses the influence of the far-plume boundary condition. Figure 12 compares the computed frequencies at the channel midline for two cases. The first case sets  $T_e=1$  eV at the horizontal and vertical far-plume boundaries (see Figure 1) and the second case sets  $T_e=4$  eV at these boundaries. As expected, the near-plume and channel regions are not found to be significantly affected whereas the far-plume regions are largely driven by the boundary value. Recent plasma measurements in the far-plume regions indicate that the temperature several channel heights downstream of the exit is 4-5 eV.<sup>41</sup> A value of 4 eV has been used for the BPT-4000 benchmark simulations shown in Figure 7 and Figure 8. The results in Figure 11 on the effects of  $\alpha$  were obtained with  $T_e=1$  eV at the far-plume boundaries and the qualitative trends associated with e-i collision frequency are found to be unaffected by this value. The ensuing simulations with the 6 kW Hall thruster use  $T_e=4$  eV at the boundaries based on recent plasma measurements.<sup>14</sup>

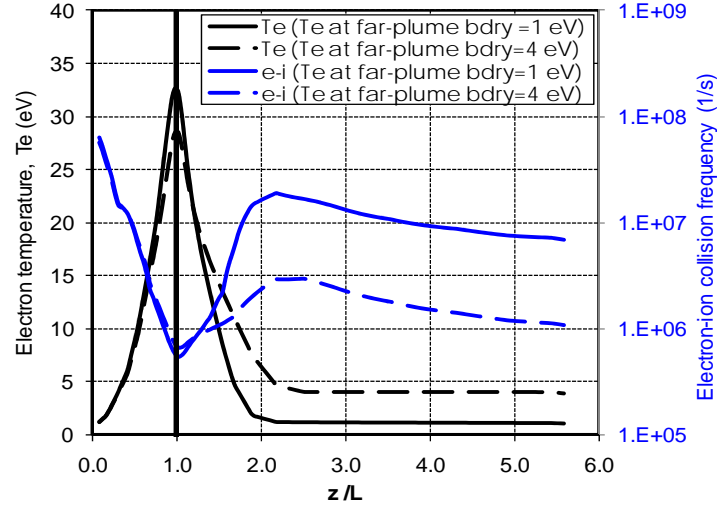


**Figure 10. Left: The response of the classical e-i collision frequency to reductions of the imposed Bohm collision frequency (through the Bohm factor  $\alpha$ ) along a line at the middle of the acceleration channel. Right: The computed anode and beam currents as a function of time for  $\alpha=0.2$ .**



**Figure 11. The response of the Hall parameter  $\Omega_e$  (left) and the electron temperature (right) to reductions of the imposed Bohm collision frequency (through the Bohm factor  $\alpha$ ) along a line at the middle of the acceleration channel.**



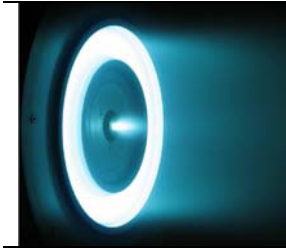


**Figure 12. Sensitivity of the electron-ion collision frequency on the far-plume boundary conditions for the electron temperature.**

### B. Extended simulations with the 6-kW laboratory Hall thruster

In this section we extend the studies of Section III.A on the effects of reduced Bohm collision frequency to a 6 kW laboratory Hall thruster. This thruster has a simpler channel geometry compared to the BPT-4000, and is being operated and studied for fundamental research at several institutions.<sup>40,42,43,44</sup> Also, several measurements have been obtained with the cathode placed at the axis of symmetry<sup>40</sup> (e.g. see photo in Table 2). This cathode-thruster arrangement is of great interest in numerical simulations because it is 2-D axisymmetric. The operational characteristics for the simulations presented in this paper are outlined in Table 2. The magnetic field arrangement, physical domain and field-aligned computational mesh are shown in Figure 13.

**Table 2. Operational characteristics used in the numerical simulations of the 6 kW laboratory Hall thruster.**

	Thruster parameter	Value
	Discharge (or anode) current (A)	20
	Discharge voltage (V)	300
	Anode mass flow rate (mg/s)	20.98
	Cathode mass flow rate (mg/s)	1.47

The solid curves in Figure 14 depict the Hall 2De solution with a reduction of the Bohm collision frequency and Hall parameter in the far-plume similar to that implemented in the BPT-4000 simulations. It is found that the maximum value of  $\alpha$ , with the prescribed spatial arrangement shown by the solid curve in Figure 14, that yields the observed anode current is 0.4. These set of simulation results have been obtained to allow for direct comparisons with ensuing simulations that lift the constraints on  $v_B$  and  $\Omega_e$ . The computed anode current and beam currents are shown in Figure 14-right. Due to their small impact on studies related to the collision frequencies the  $\text{Xe}^{+++}$  have been excluded from these simulations. The singly- and doubly-charged ion beam currents are  $I^+=13.7$  A and  $I^{++}=4.6$  A. The computed profile for  $T_e$  appears to be in fair agreement with the measurements as suggested by Figure 15-right (solid curve).

The dashed curves in Figure 14 illustrate the corresponding results when  $v_B$ ,  $\Omega_e$  and all other plasma variables are determined self-consistently with no spatial restrictions on  $\alpha$  in the far-plume. The motivation for these simulations is not to imply that anomalous (Bohm) diffusion extends to the far-plume; here we aim to demonstrate the effect that the *ad-hoc* elimination of the Bohm collision frequency and Hall parameter has on the plasma solution. The proposed implication is that in models such as HPHall the inherent limitations posed by the quasi-1D assumption on the extent of the computational domain make the achievement of a numerical solution that is unbiased by the imposed restrictions beyond the near-cathode line (see Figure 6) challenging if not impossible. The

relatively small differences between the two simulation cases for the integrated variables such as anode and beam currents (see Figure 14-right) falsely imply a small effect by the imposed restrictions. But the comparisons for the electron temperature do not support such assertions. Figure 15-right quantifies the different spatial extents associated with the diffusion of heat in the electron flow along the channel midline for the two cases, and Figure 16 compares the 2-D profiles.

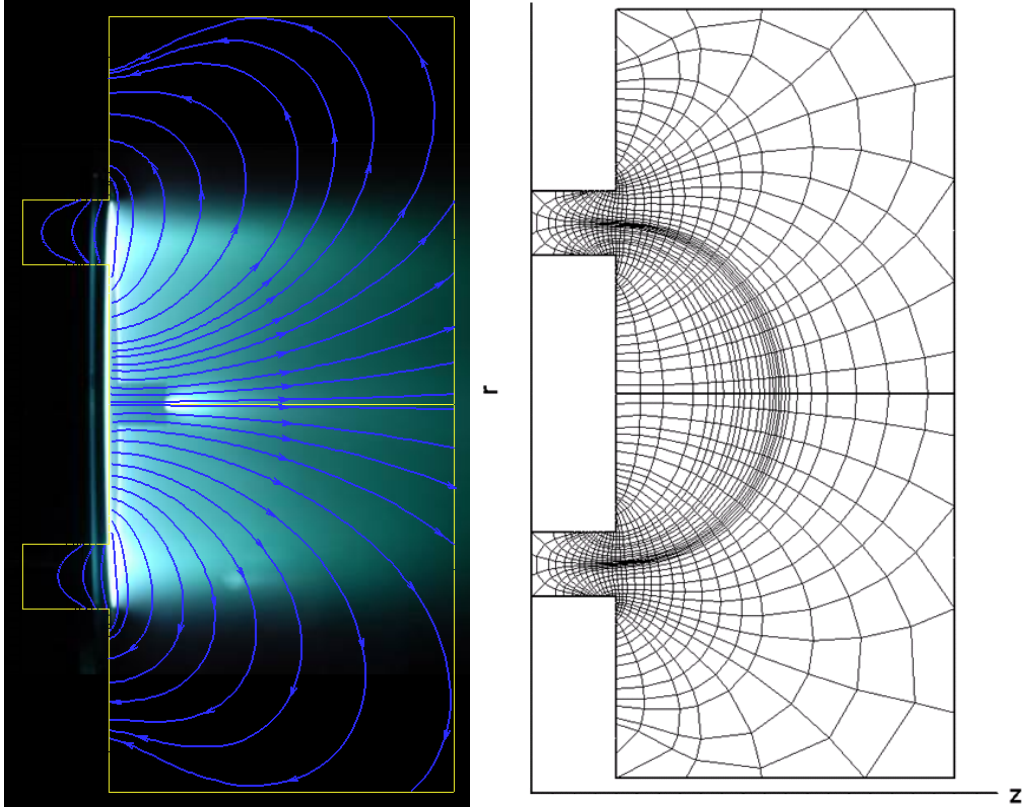


Figure 13. Physical domain, magnetic field and computational mesh for the numerical simulations of the 6 kW laboratory Hall thruster.

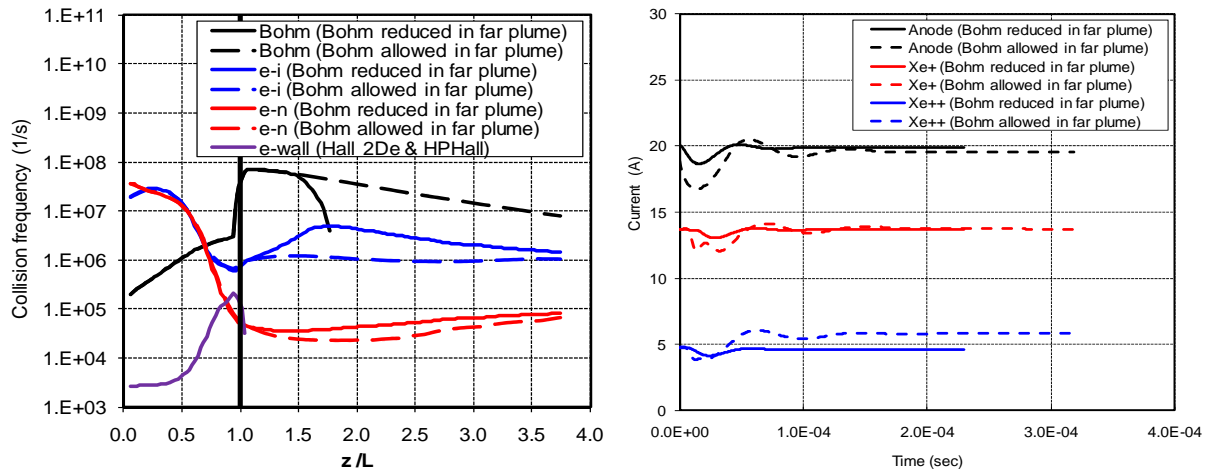


Figure 14. Studies on the effect of reducing the Bohm collision frequency and the Hall parameter in the far plume (case shown is for a maximum Bohm factor of  $\alpha=0.4$ ). Left: Collision frequencies along the middle of the channel. Right: Anode and beam currents as a function of numerical simulation time.

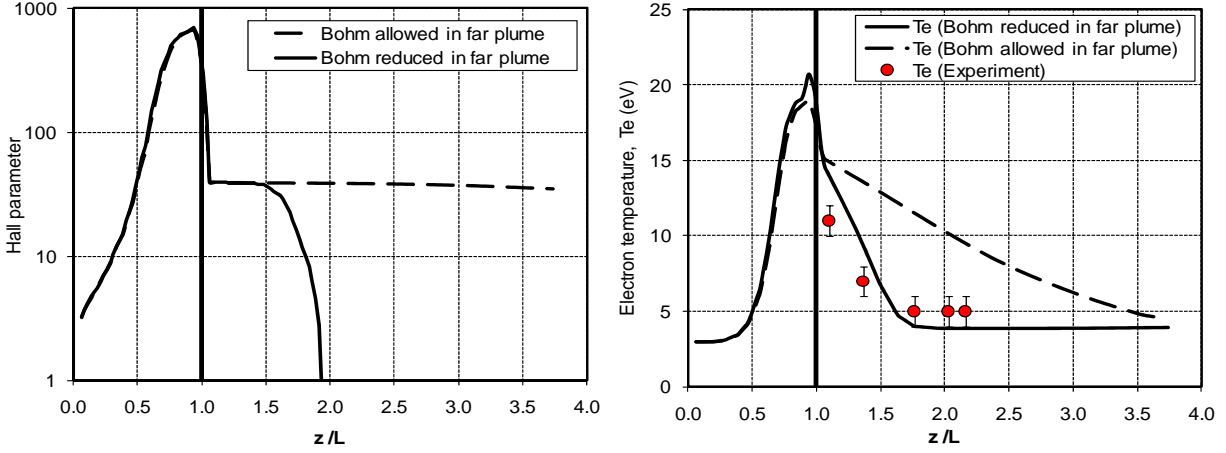


Figure 15. Studies on the effect of reducing the Bohm collision frequency and the Hall parameter in the far plume (case shown is for a maximum Bohm factor of  $\alpha=0.4$ ). The plots compare solutions along the middle of the channel.

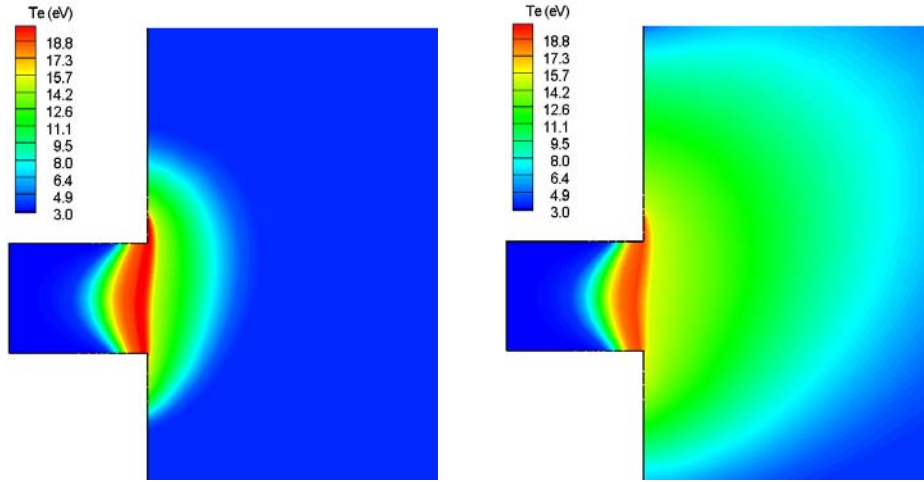


Figure 16. Studies on the effect of reducing the Bohm collision frequency and the Hall parameter in the far plume (case shown is for a maximum Bohm factor of  $\alpha=0.4$ ). The plots compare 2-D contours of the electron temperature. Left:  $v_B$  and  $\Omega_e$  reduced beyond  $z/L \sim 1.5$ . Right: No reductions of  $v_B$  and  $\Omega_e$  in the far plume.

A related result is in Figure 17, which shows 2-D contours of the Hall parameter overlaid by unit vectors of the electron flux for the case of no reductions of  $\alpha$  in the far-plume region. Selected streamlines of the magnetic field are also shown. The plot suggests the formation of an effective “funneling region” for the electrons that extends far beyond the end of the HPHall computational region. The regions of lowest Hall parameter are closely aligned with the ion beam as shown in Figure 17-right; this is where the drag force density  $\mathbf{R}_e$  on the electrons has the largest contributions by the classical e-i collision frequency. However, because the Bohm collision for this case remains the dominant frequency throughout the plume region, the precise electron paths especially in the areas near the magnets (i.e. the “lobes” of high Hall parameter shown in Figure 17) cannot yet be identified.

The proximity of the values of the two collision frequencies, e-i and Bohm, in the far-plume regions and the apparent insignificance of the latter in most of the acceleration channel motivated the next series of numerical simulations. In these simulations we aim to eliminate the Bohm collision frequency inside the channel while lowering the value of  $\alpha$  in the plume even further. Two cases are compared in Figure 18-left and Figure 19-left corresponding to two values of the Bohm factor:  $\alpha=0.15$  and  $\alpha=0.075$ . The Bohm collision frequency inside the channel for both cases has been eliminated as shown in Figure 19-left. The comparison with plasma measurements for the case of  $\alpha=0.15$  is shown Figure 19-right. As in the BPT-4000 cases, it is found that by reducing  $v_B$  in the plume region the damping of the low-frequency oscillations is also diminished. Figure 18-right shows oscillations in

the computed currents with a frequency of  $\sim 8.5$  kHz, which is about 2.5 times lower than the observed value of  $\sim 20$  kHz.<sup>14,36</sup> The average anode current in both cases is also lower than the observed value, by  $\sim 3.5$  A.

These simulations combined with the previous results on the BPT-4000 illustrate clearly the dependence of the spatial and temporal parts of the solution on the magnitude and spatial distribution chosen for the Bohm collision frequency. Presently, this marked dependence renders extended comparisons with time-averaged plasma measurements and thruster performance useful only in terms of broad guidance on further studies related to electron transport. Thus far, the trends from all the preliminary simulations in this paper suggest that lowering  $\alpha$  even further may increase the amplitude of the low-frequency oscillations but the effect on the time-averaged currents is not yet known. Also, Figure 17-left suggests that lowering  $\alpha$  further could have a significant effect on the funneling of electrons from the plume regions, especially in relation to the expected increase of the Hall parameter near the magnets and the diffusion of electrons in these regions. Further studies on  $\alpha$  are planned as part of the development and validation of Hall 2De.

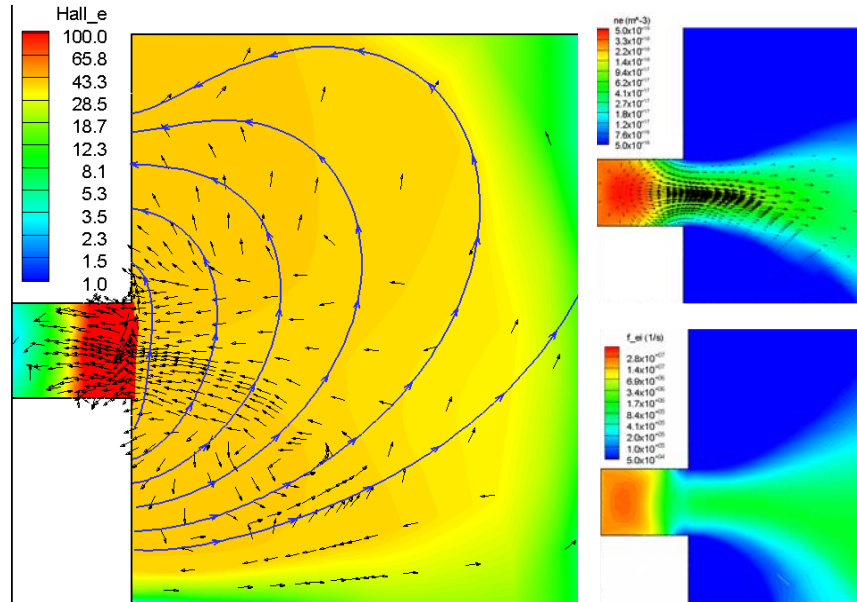


Figure 17. Left: contours of the Hall parameter overlaid by unit vectors of the electron particle flux and by selected streamlines of the magnetic field (shown in blue). Right-top: contours of the electron number density overlaid by the singly-charged ion velocity field. Right-bottom: contours of the e-i collision frequency.

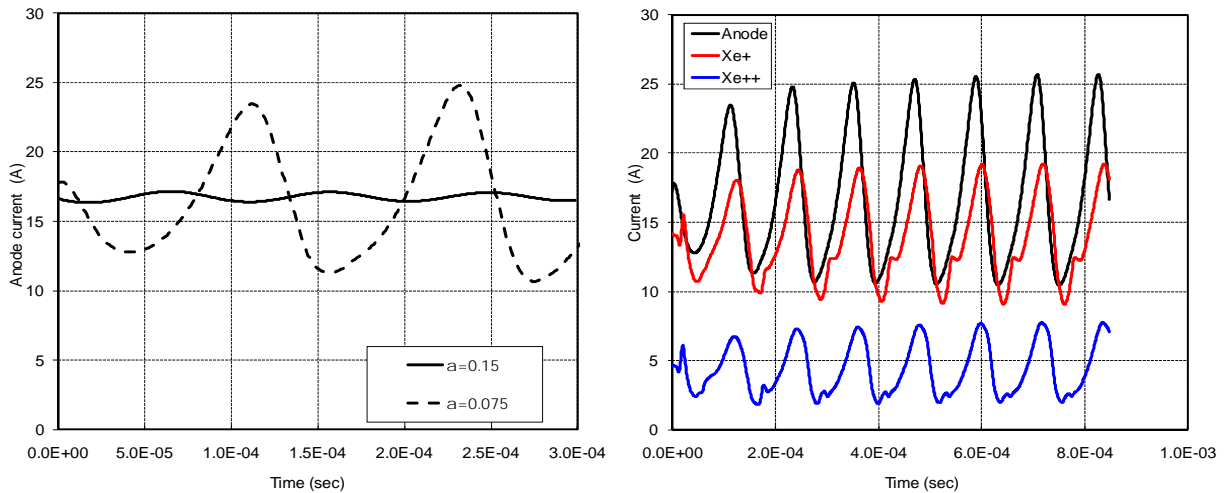
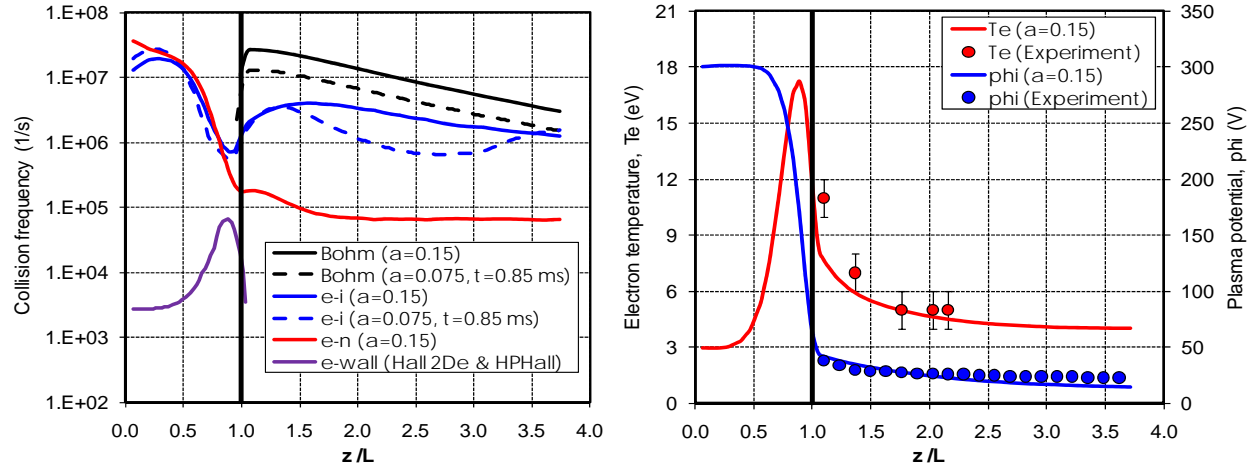


Figure 18. Numerical simulations of the 6 kW Hall thruster with no Bohm diffusion inside the acceleration channel. Left: anode current for two values of  $\alpha$ : 0.15 and 0.075. Right: anode and beam currents for  $\alpha = 0.075$  (showing longer simulation time).



**Figure 19. Numerical simulations of the 6 kW Hall thruster with no Bohm diffusion inside the acceleration channel. Left: e-i and Bohm collision frequencies are compared for two values of  $\alpha$ : 0.15 and 0.075. Right: comparisons with plasma measurements along the middle of the acceleration channel for the case of  $\alpha=0.15$ .**

#### IV. Conclusion

This paper has reported on the development of a 2-D axisymmetric computational model for Hall thrusters that has the following main features: (1) resolution of electron transport parallel and perpendicular to the magnetic field, made possible by the discretization of the electron fluid equations on a field-aligned mesh, (2) implicit solution for the conduction of electron current and heat, (3) large computational region (by comparison to state-of-the-art hybrid simulation models) that extends several times the channel size downstream of the thruster exit, (4) solution of the hydrodynamic equations of continuity and momentum for isothermal ions, accounting for multiple ionization and charge-exchange collisions with neutrals, (5) an algorithm for the (collisionless) neutral gas that does not depend on discrete particles. Features (4) and (5) allow for “quiet” simulations of Hall thrusters by eliminating the statistical noise that is inherent in discrete-particle methods,

Results from a first series of simulations of the BPT-4000 and of a 6 kW laboratory Hall thruster suggest that the anode region is dominated by ion diffusion with the electric field predicted to be negligibly small there. The results show a significantly higher plasma density in this region by comparison to the hybrid simulation results of HPHall. Studies to assess the importance of the Bohm collision frequency (that is usually imposed in the HPHall simulations) on the spatial and temporal behavior of the plasma suggest that the solution is not insensitive to the conditions imposed beyond the near-cathode magnetic field line. Although it has been known (at least for the two thrusters studied here) that the imposed spatial distribution of the Bohm collision frequency in HPHall has a significant effect on the plasma solution in the vicinity of the channel exit, the significance of the conditions imposed downstream of the near-cathode streamline could not be assessed due, in part, to the limited extent of the HPHall domain. By solving for the electron flow with the Hall 2De extended region it is found that the flow field exhibits characteristics that are purely two-dimensional and cannot be resolved with a quasi-one-dimensional electron model. In regards to the temporal behavior of the solution it is found that the Bohm collision frequency also influences significantly the damping of the current oscillations. If lowered sufficiently, to values that near the e-i collision frequency in regions of the plume, only then does the plasma begin to exhibit the temporal behavior that is known to persist in Hall thrusters (the well-known “breathing mode”). It has been hypothesized in this paper that the damping of these oscillations computed at the high-Bohm values is due to its dominance over all other collision frequencies; the first is independent of the plasma conditions whereas the second is not and can therefore participate in transient plasma behavior. Although the questions on turbulence and its significance on the transport of electrons remain unanswered by the simulation results presented herein, it appears that the path to the answer cannot exclude the two-dimensional character of the electron flow field in the thruster plume.

## Acknowledgments

The research described in this paper was carried out by the Jet Propulsion Laboratory, California Institute of Technology, under a contract with the National Aeronautics and Space Administration. Reference herein to any specific commercial product, process, or service by trade name, trademark, manufacturer, or otherwise, does not constitute or imply its endorsement by the United States Government or the Jet Propulsion Laboratory, California Institute of Technology.

## References

- <sup>1</sup> Morozov, A. I., *Plasma Accelerators*, ed. Archimovich L. A., M. Mashinostroenie, 1973, p. 5-15, 85-92 (in Russian).
- <sup>2</sup> Morozov, A. I., Melikov I. V., *Journal of Technical Physics*, 1974, v. 44, No. 3, p. 544 (in Russian).
- <sup>3</sup> Volkov, B. I., Morozov A. I., Sveshnikov A. G., Yakunin C. A., preprint Kurchatov Inst. Atomic Energy, No. 2945, M. 1978 (in Russian).
- <sup>4</sup> Hirakawa, M. and Arakawa, Y., "Particle Simulation of Plasma Phenomena in Hall Thrusters," 24<sup>th</sup> International Electric Propulsion Conference, IEPC Paper 1995-164, Moscow, Russia, 1995.
- <sup>5</sup> Hirakawa, M. and Arakawa, Y., "Numerical Simulation of Plasma Particle Behavior in a Hall Thruster," 32<sup>nd</sup> AIAA Joint Propulsion Conference, AIAA Paper 1996-3195, Lake Buena Vista, FL, 1996.
- <sup>6</sup> Hirakawa, M., "Electron Transport Mechanism in a Hall Thruster," 25<sup>th</sup> International Electric Propulsion Conference, IEPC Paper 1997-021, Cleveland, OH, 1997.
- <sup>7</sup> Fife, J. M., "Hybrid-PIC Modeling and Electrostatic Probe Survey of Hall Thrusters," Ph.D. Thesis, Aeronautics and Astronautics, Massachusetts Institute of Technology, 1998.
- <sup>8</sup> Fife, J. M., Martinez-Sanchez, M., and Szabo, J., "A Numerical Study of Low-Frequency Discharge Oscillations in Hall Thrusters," 33<sup>rd</sup> AIAA/ASMA/SAE/ASEE Joint Propulsion Conference, Seattle, WA, 1997.
- <sup>9</sup> Boeuf, J. P., and Garrigues, L., "Low Frequency Oscillations in a Stationary Plasma Thruster," *Journal of Applied Physics*, **84**, 7, p. 3541, 1998.
- <sup>10</sup> Bohm, D., Burhop, E., and Massey, H., *Characteristics of Electrical Discharges in Magnetic Fields*, ed. Guthrie, A. and Waterling, R. K., Eds., McGraw-Hill, New York, 1949.
- <sup>11</sup> Parra, F. I., Ahedo, E., Fife, J. M., and Martinez-Sanchez, M., "A Two-Dimensional Hybrid Model of the Hall Thruster Discharge," *Journal of Applied Physics*, **100**, 023304 (2006).
- <sup>12</sup> Gamero-Castaño, M. and Katz, I., "Estimation of Hall Thruster Erosion Using HPHall," 29<sup>th</sup> International Electric Propulsion Conference, IEPC Paper 2005-303, Princeton, NJ, 2005.
- <sup>13</sup> Hofer, R. R., Mikellides, I. G., Katz, I., and Goebel, D. M., "BPT-4000 Hall Thruster Discharge Chamber Erosion Model Comparison with Qualification Life Test Data," 30<sup>th</sup> International Electric Propulsion Conference, IEPC Paper 2007-267, Florence, Italy, 2007.
- <sup>14</sup> Hofer, R. R., Katz, I., Mikellides, I. G., Goebel, D. M., Jameson, K. K., Sullivan, R. M., and Johnson, L. K., "Efficacy of Electron Mobility Models in Hybrid-PIC Hall Thruster Simulations," 44<sup>th</sup> AIAA Joint Propulsion Conference, AIAA Paper 2008-4924, Hartford, CT, 2008.
- <sup>15</sup> Fernandez, E., Cappelli, M. A., and Mahesh, K., "2-D simulations of Hall thrusters," in *CTR Annual Research Briefs*. Palo Alto, CA: Stanford Univ., 1998, p. 81.
- <sup>16</sup> Sommer, E., Scharfe, M. K., Gascon, N., Cappelli, M. A., and Fernandez, E., "Simulating Plasma-Induced Hall Thruster Wall Erosion With a Two-Dimensional Hybrid Model," *IEEE Transactions on Plasma Science*, **35**, 5, p. 1379, 2007.
- <sup>17</sup> Hagelaar, G., Bareilles, J., Garrigues, L., and Boeuf, J. P., "Two Dimensional Model of a Stationary Plasma Thruster," *Journal of Applied Physics*, **91**, p. 5592, 2002.
- <sup>18</sup> Bareilles, J., Hagelaar, G., Garrigues, L., Boniface, C., and Boeuf, J., "Critical Assessment of a Two-Dimensional Hybrid Hall Thruster Model: Comparisons with Experiments," *Physics of Plasmas*, **11**, 6, 2004.
- <sup>19</sup> Garrigues, L., Hagelaar, G. J., Boniface, C., and Boeuf, J. P., "Anomalous Conductivity and Secondary Electron Emission in Hall Effect Thrusters," *Journal of Applied Physics*, **100**, 123301, 2006.
- <sup>20</sup> Morozov, A. I. and Savelyev, V. V., "Numerical Simulation of Plasma Flow Dynamics in SPT," 24<sup>th</sup> International Electric Propulsion Conference, IEPC Paper 1995-161, Moscow, Russia, 1995.
- <sup>21</sup> Morozov A. I., and Savelyev, V. V., "Fundamentals of Stationary Plasma Thruster Theory," *Reviews of Plasma Physics*, **21**, p. 203, 2000.



- <sup>22</sup> Keidar, M., Boyd, I. D., and Beilis, I. I., "Plasma Flow and Plasma–Wall Transition in Hall Thruster Channel," *Physics of Plasmas*, **8**, 12, pp. 5315-5322, 2001.
- <sup>23</sup> Mikellides, I. G., Katz, I., Goebel, D. M., Jameson, K. K., and Polk, J. E., "Wear Mechanisms in Electron Sources for Ion Propulsion, II: Discharge Hollow Cathode," *Journal of Propulsion and Power*, **24**, 4, pp. 866-879, 2008.
- <sup>24</sup> Mikellides, I. G., and Katz, I., "Wear Mechanisms in Electron Sources for Ion Propulsion, I: Neutralizer Hollow Cathode," *Journal of Propulsion and Power*, **24**, 4, pp. 855-865, 2008.
- <sup>25</sup> Marchand R., and Dumbergy, M., "CARRE: A Quasi-Orthogonal Mesh Generator for 2D Edge Plasma Modeling," *Computer Physics Communications*, **96**, pp. 232-246, 1996.
- <sup>26</sup> Lin, Z., Hahm, T. S., Lee, W. W., Tang, W. M., and White, R. B., "Turbulent Transport Reduction by Zonal Flows: Massively Parallel Simulations," *Science*, **281**, pp. 1835-1837, 1998.
- <sup>27</sup> Dimits, A. M., "Fluid Simulations of Tokamak Turbulence in Quasiballoonning Coordinates," *Physical Review E*, **48**, pp. 4070-4079, 1993.
- <sup>28</sup> LeBrun, M. J., Tajima, T., Gray, M. G., Furnish, G., and Horton, W., "Toroidal Effects on Drift Wave Turbulence," *Physics of Fluids B*, **5**, 3, pp. 752-773, 1993.
- <sup>29</sup> Marchand, R., Lu, J. Y., Kabin, K., and Rankin, R., "Unstructured Meshes and Finite Elements in Space Plasma Modelling: Principles and Applications," in *Advanced Methods for Space Simulations*, eds Usui, H. and Omura, Y., Terrapub, Tokyo, pp. 111–143, 2007.
- <sup>30</sup> Wirz R., Katz I., 'A Preliminary 2-D Computational Model of an Ion Thruster Discharge Chamber', 39th AIAA Joint Propulsion Conference, AIAA Paper 2003-5163, Huntsville, AL, 2003.
- <sup>31</sup> Wirz, R. E., "Discharge Plasma Processes of Ring-Cusp Ion Thrusters," Ph.D. Dissertation, Aeronautics, Caltech, Pasadena, CA, 2005.
- <sup>32</sup> Katz, I., and Mikellides, I. G., "A New Algorithm for the Neutral Gas in the Free-Molecule Regimes of Hall and Ion Thrusters," 31<sup>st</sup> International Electric Propulsion Conference, IEPC Paper 2009-95, Ann Arbor, MI, 2009.
- <sup>33</sup> Huang, W., Drenkow, B., and Gallimore, A. D., "Laser-Induced Fluorescence of Singly-Charged Xenon Inside a 6-kW Hall Thruster," 45<sup>th</sup> AIAA Joint Propulsion Conference, AIAA Paper 2009-5355, Denver, CO, 2009.
- <sup>34</sup> Miller, J. S., Pullins, S. H., Levandier, D. J., Chiu, Y., Dressler, R. A., "Xenon Charge Exchange Cross Sections for Electrostatic Thruster Models," *Journal of Applied Physics*, **91**, 3, pp. 984-991, 2002.
- <sup>35</sup> Zumdahl, S., *Chemistry*, D. C. Heath & Co., p. 280, 1986.
- <sup>36</sup> Reid, B. M. and Gallimore, A. D., "Langmuir Probe Measurements in the Discharge Channel of a 6-kW Hall Thruster," 44<sup>th</sup> AIAA Joint Propulsion Conference, AIAA Paper 2008-4920, Hartford, CT, 2008.
- <sup>37</sup> Braginskii, S. I., "Transport Processes in Plasmas," *Reviews of Plasma Physics*, Vol. 1, edited by M. A. Leontovich, Consultants Bureau, New York, 1965, pp. 205–311.
- <sup>38</sup> Hobbs, G. D. and Wesson, J. A., "Heat Flow Through a Langmuir Sheath in the Presence of Electron Emission," *Plasma Physics*, **9**, pp. 85-87, 1967.
- <sup>39</sup> Hofer, R. R., Mikellides, I. G., Katz, I., and Goebel, D. M., "Wall Sheath and Electron Mobility Modeling in Hybrid-PIC Hall Thruster Simulations," 43<sup>rd</sup> AIAA Joint Propulsion Conference, AIAA Paper 2007-5267, Cincinnati, OH, 2007.
- <sup>40</sup> Reid, B. M., "The Influence of Neutral Flow Rate in the Operation of Hall Thrusters," Ph.D. Thesis, Aerospace Engineering, University of Michigan, 2009.
- <sup>41</sup> Private communication with D. M. Goebel. Data not yet published.
- <sup>42</sup> Brown, D. L., Larson, C. W., Haas, J. M., and Gallimore, A. D., "Analytical Extraction of Plasma Properties Using a Hall Thruster Efficiency Architecture," 30<sup>th</sup> International Electric Propulsion Conference, IEPC Paper 2007-188, Florence, Italy, 2007.
- <sup>43</sup> Shastry, R., Hofer, R. R., Reid, B. M., and Gallimore, A. D., "Method for Analyzing ExB Probe Spectra from Hall Thruster Plumes," *Review of Scientific Instruments*, **80**, 063502, 2009.
- <sup>44</sup> Jameson, K. K., "Investigation of Hollow Cathode Effects on Total Thruster Efficiency in a 6 kW Hall Thruster," Ph.D. Dissertation, Aerospace Engineering, University of California, Los Angeles, 2008.